M 2022

U.PORTO
FEUP FACULDADE DE ENGENHARIA
UNIVERSIDADE DO PORTO

ANALYSIS OF NATURAL VENTILATION IN PRIMARY CLASSROMS USING CFD

EDUARDO ROSAS GARCEZ LENCASTRE
MASTER THESIS IN CHEMICAL ENGINEERING
PRESENTED TO THE FACULTY OF ENGINEERING
OF THE UNIVERSITY OF PORTO

Master in Chemical Engineering

Analysis of Natural Ventilation in Primary Classrooms using CFD

Master dissertation

of

Eduardo Rosas Garcez Lencastre

Developed within the course of dissertation

held in

LEPABE – Laboratory for Processes Engineering, Environment, Biotechnology and Energy

LSRE-LCM - Laboratory of Separation and Reaction Engineering – Laboratory of Catalysis and Materials

ALiCE – Associate Laboratory in Chemical Engineering







Supervisor at FEUP: Margarida Sarmento e Cunha Abrunhosa de Brito, PhD

Joint supervisor at FEUP: Sofia Isabel Vieira de Sousa, PhD





July 2022

Acknowledgment

Em primeiro lugar, queria agradecer à minha orientadora, Margarida Brito por toda a ajuda, disponibilidade e apoio que me deu que foram fundamentais para a realização deste trabalho.

Gostaria também de agradecer ao Professor Ricardo Santos, bem como à minha coorientadora, Sofia Sousa, por todos os ensinamentos e recomendações tão importantes.

De seguida, gostaria de agradecer aos colegas que de uma forma ou outra, ajudaram na construção deste trabalho. Em especial, ao Mateus Caixeta, pela ajuda e disponibilidade na construção das malhas 3D.

Não posso de deixar de agradecer ao LSRE-LCM pela oportunidade de contribuir para o projeto 2SMART.

Queria agradecer também a todos os meus colegas de curso, em especial à Catarina, à Inês e à Luana, que me acompanharam durante o curso e cujo apoio e amizade me ajudaram neste percurso.

À minha família, Pais, irmãos e restantes familiares que sempre me encorajaram e apoiaram em todas as etapas da minha vida.

Por fim agradeço a todos os meus amigos ainda não mencionados que direta ou indiretamente me ajudaram na realização desta tese.

This work was financially supported by LA/P/0045/2020 (ALiCE), UIDB/00511/2020 and UIDP/00511/2020 (LEPABE), and UIDB/50020/2020 and UIDP/50020/2020 (LSRE-LCM) funded by national funds through FCT/MCTES (PIDDAC); Project PTDC/EAM-AMB/32391/2017 - POCI-01-0145-FEDER-032391, funded by FEDER funds through COMPETE2020 – Programa Operacional Competitividade e Internacionalização (POCI) and by national funds (PIDDAC) through FCT/MCTES; and Project 2SMART - engineered Smart materials for Smart citizens, with reference NORTE-01-0145-FEDER-000054, supported by Norte Portugal Regional Operational Programme (NORTE 2020), under the PORTUGAL 2020 Partnership Agreement, through the European Regional Development Fund (ERDF).

Abstract

Indoor Air Quality has an enormous impact on our daily lives since it significantly affects our health, well-being, and comfort. Since, in the last few decades, the time that people spend indoors has significantly increased the interest in understanding this type of environment, namely regarding to indoor air quality, has been increasingly studied.

In this work two approaches were performed: first using a simplified 2D CFD domain and second a more complex full 3D CFD domain. The effect of some of the simulation setup conditions on the converged solution were analysed as well as some design parameters for the optimization of wind-driven ventilation of a classroom, namely, the volume of the room, the window dimensions, and the wind speed. The ventilation power was studied using tracer simulations, using CO_2 has the tracer gas.

It was found that the wall roughness and the inlet turbulence conditions didn't affect the solution. The shape of the flow through the window, was described by the bottom and middle of the window (70%) serving as an inlet, while from the top part and sides of the window, the other 30%, the air leaves the room in a shape of a jet. The results showed that out-flowrate is linearly correlated with the wind speed. However, the same relation is not observed when changing the opening area. It was also found that the distance of the window to the room's walls played a significant effect on the ventilation.

With the tracer simulations it was found that only a fraction of the flowrate, $\%Q_{eff}$, (15% to 25% for 2D simulations and 35% to 45% for 3D simulations) contributed to the effective renewal of the indoor air. It was also found that the ventilation could modelled by the Danckwerts $F(t)$ curve for CSTR. The results also showed that the air is renewed mainly by turbulent dispersion rather than convection.

Keywords (theme): **N**atural ventilation, Wind-driven ventilation, indoor air quality and CFD

Resumo

A qualidade do ar interior tem um enorme impacto no nosso dia-a-dia, uma vez que afeta significativamente a nossa saúde, bem-estar e conforto. Nas últimas décadas, o tempo que as pessoas passam dentro de casa tem aumentado significativamente. Assim, o interesse em compreender este tipo de ambiente, nomeadamente no que diz respeito à qualidade do ar interior, tem sido cada vez maior.

Neste trabalho foram realizadas duas abordagens: primeiro utilizando um domínio 2D CFD simplificado e em segundo lugar um domínio 3D CFD mais complexo. Foram analisados os efeitos de algumas das condições de configuração da simulação na solução convergida, bem como alguns parâmetros de design para a otimização da ventilação impulsionada pelo vento de uma sala de aula, nomeadamente, o volume da sala, as dimensões das janelas e a velocidade do vento. A potência de ventilação foi estudada usando simulações de tracer, utilizando CO_2 como o gás de estudo.

Verificou-se que a rugosidade da parede e as condições de turbulência da entrada não afetaram a solução. A forma do escoamento através da janela foi descrita como, entrada de ar pelo fundo e meio da janela (70%), enquanto que na parte superior e os lados da janela, os outros 30%, o ar sai da sala em forma de jato. Os resultados mostraram que o escoamento está linearmente correlacionado com a velocidade do vento. No entanto, a mesma relação não é observada quando se altera a área de abertura. A distância da janela para as paredes da sala também teve um efeito significativo na ventilação.

Com as simulações de tracer verificou-se que apenas uma fração do caudal total, $\%Q_{eff}$, (15% a 25% para simulações 2D e 35% a 45% para simulações 3D) contribuiu para a efetiva renovação do ar interior. Verificou-se também que a ventilação pode ser modelada pela função de distribuição de tempos de residência, (DTR) também conhecida como curva F de Danckwerts. Os resultados também mostraram que o ar é renovado principalmente por uma dispersão turbulenta em vez de convecção.

Declaration

I hereby declare, under word of honour, that this work is original and that all non-original contributions are indicated, and due reference is given to the author and source

Eduardo Lencastre

02/07/2022

Index

1 Introduction 1

1.1 Framing and presentation of the work 1

1.2 Contribution of the author to the work 2

1.3 Organization of the dissertation 2

2 Context and State of the art 3

2.1 Natural Ventilation 4

2.2 Computational Fluid Dynamics in Natural Ventilation Studies 5

2.2.1 Turbulence models 7

2.2.2 Natural Ventilation CFD Simulations 9

3 2D Simulation of Natural Ventilation 11

3.1 Numerical Methods Validation 11

3.1.1 Computation Domain and Solution Methodology 11

3.1.2 Mesh Independence Test 12

3.1.3 Single Sided Ventilation 13

3.1.4 Cross Ventilation 18

3.2 Ventilation Parameter Study 20

3.2.1 Effect of Wind Speed 20

3.2.2 Effect of Room Dimensions 22

3.2.3 Effect of Window Dimensions 24

3.3 CO_2 Tracer Simulations 26

3.3.1 Setup and Solution Methodology 26

3.3.2 Results and Discussion 27

4 3D Simulation of Natural Ventilation 31

4.1 3D Symmetric CFD model 31

4.1.1 Comparison with RNG model 34

4.2 3D CFD Simulation – Full domain 34

4.2.1 Mesh Independence test 35

4.2.2 Results and discussion 36

4.3 CO_2 Tracer Simulations 40

5 Conclusions 45

6 Assessment of the work done 47

6.1 Objectives Achieved 47

6.2 Future Work 47

7 References 48

Appendix A - Extra Tracer Simulation li

Appendix B – Exterior Flow Structure liii

List of Figures

Figure 1. Geometry and mesh of the 2D domain. *11*

Figure 2. x*-velocity profile at the window for single sided ventilation determined from 2D CFD model.* *14*

Figure 3. Streamlines for single sided ventilation: full domain (top); indoor (bottom) determined from 2D CFD simulations *15*

Figure 4. Velocity vector field for single sided ventilation determined from 2D CFD simulations *15*

Figure 5. x*-velocity profiles determined from 2D CFD simulations for different Ks, using standard* k*-*ε*.* $Ks = 0\ m$ *(blue);* $Ks = 2 \times 10 - 4\ m$ *(red);* $Ks = 3 \times 10 - 4\ m$ *(squares);* $Ks = 6 \times 10 - 4\ m$ *(crosses);* $Ks = 1 \times 10 - 3\ m$ *(purple).* *16*

Figure 6. x*-velocity at the window for single sided ventilation using 2D CFD model and Standard k-ε (red); Realisable k-ε (blue); RNG (green); LES (purple).* *17*

Figure 7. x*-velocity profile at the window for* $TI = 1\ \%$ *(red),* $TI = 4\ \%$ *(blue) and* $TI = 10\ \%$ *(green) determined from 2D CFD model.* *18*

Figure 8. Streamlines for cross ventilation: full domain (top); indoor (bottom) in 2D CFD simulations. *19*

Figure 9. Velocity vector field for cross ventilation using 2D CFD simulations. *19*

Figure 10. x*-velocity profile at the window for single sided ventilation: Windward side (blue); Leeward side (red).* *20*

Figure 11. Sketch of the window and the geometric parameters and wind speed studied in 2D CFD simulation. *20*

Figure 12. x*-velocity at the window for single sided ventilation and* $U = 5\ km\ h - 1$*(blue);* $U = 9\ km\ h - 1$*(red);* $U = 10\ km\ h - 1$ *(green);* $U = 11.6\ km\ h - 1$*(purple)* *21*

Figure 13. Normalized x*-velocity at the window for single sided ventilation and different* U*.* *22*

Figure 14. x*-velocity at the window for single sided ventilation and* $L = 3\ m$ *(blue);* $L = 4\ m$ *(orange);* $L = 5\ m$ *(gray);* $L = 5.95\ m$ *(yellow)* *23*

Figure 15. x*-velocity at the window for single sided ventilation and* $H = 3\ m$ *(blue);* $H = 3.2\ m$ *(orange)* *23*

Figure 16. x*-velocity at the window for single sided ventilation and* $w = 0.6\ m$ *(blue);* $b = 1\ m$ *(orange);* $w = 1.5\ m$ *(green)* *24*

Figure 17. x*-velocity at the window for single sided ventilation and:* $b = 0.3\ m$ *(blue);* $b = 0.1\ m$ *(red);* $b = 0.01\ m$ *(green);* $b = 0.2\ m$ *(purple);* $b = 0.4\ m$ *(cyan);* $b = 0.5\ m$ *(orange).* *25*

Figure 18. Average CO_2 *mass fraction history for the base case.* $U = 5\ km\ h - 1$ *and* $w = 0.6\ m$ *27*

Figure 19. Danckwerts $F(t)$ curve for $U = 9\ km\ h-1$, $w = 0.6\ m$. From a 2D simulation 29

Figure 20. Danckwerts $F(t)$ curve for $U = 5\ km\ h-1$, $w = 1.5\ m$. From a 2D simulation 29

Figure 21. Danckwerts $F(t)$ curve for $U = 11.6\ km\ h-1$, $w = 0.6\ m$. From a 2D simulation..... 30

Figure 22. Mass fraction of CO_2, $xCO2$, contour map for the base case at $t = 30\ min$. 30

Figure 23. 3D CFD geometry considering half of the physical domain. 31

Figure 24. Front view of 3D half geometry. 32

Figure 25. x-velocity profile at $z = 10\ m$: 2D (green); Mesh 3DS_2M (blue) for 3D symmetric domain simulation. case ($U = 5\ km\ h-1$, $w = 0.6\ m$). 33

Figure 26. x-velocity profile at $y = 2.4\ m$ for a 3D symmetric domain simulation. case ($U = 5\ km\ h-1$, $w = 0.6\ m$). 34

Figure 27. 3D Geometry for the full domain. 35

Figure 28. 3D Geometry for the full domain. Front view..... 35

Figure 29. x-velocity profile of $z = 10\ m$, from 3D simulations: 3DF_3M (blue); 3DS_2M (cyan)..... 37

Figure 30. x-velocity profile at $y = 2.4\ m$. from 3D simulation of full domain 37

Figure 31. x-velocity profile of the window at $z = 10\ m$: Standard k-ε model (blue); RNG model (orange). 38

Figure 32. x-velocity profile at at $y = 2.4\ m$: Standard k-ε model (blue); RNG model (orange). 38

Figure 33. x-velocity contour at the window from a 3D simulation..... 39

Figure 34. x-velocity contour map at the window for $s = 2\ m$ for a 3D simulation 40

Figure 35. Danckwerts $F(t)$ curve for the base case ($U = 5\ km\ h-1$, $w = 0.6\ m$). From a 3D simulation. 41

Figure 36 Danckwerts $F(t)$ curve for $U = 9\ km\ h-1$ from a 3D CFD simulation. 42

Figure 37. Danckwerts $F(t)$ curve for $U = 11.6\ km\ h-1$ from a 3D CFD simulation. 42

Figure 38. Danckwerts $F(t)$ curve for $w = 1.5\ m$ from a 3D CFD simulation. 43

Figure 39. Average CO_2 mass fraction history for the base case, . $U = 5\ km\ h-1$ and $w = 0.6\ m$, and an initial concentration of 0.025 from a 2D simulation (right) and a 3D simulation (left) li

Figure 40 Average CO_2 mass fraction history for from a 2D simulation and an initial concentration of 0.003. $U = 9\ km\ h-1$ and $w = 0.6\ m$ lii

Figure 41. Front view of pathlines coloured by velocity magnitude for the 3D simulation ($w = 0.6\ m$ and $U = 5\ km\ s-1$) liii

Figure 42. Back view of pathlines coloured by velocity magnitude for the 3D simulation ($w = 0.6\ m$ and $U = 5\ km\ s-1$)..... liv

Figure 43. Top view of pathlines coloured by velocity magnitude for the 3D simulation ($w = 0.6\ m$ and $U = 5\ km\ s-1$)..... liv

Figure 44. Pathlines originating from the opening of the room coloured by velocity magnitude for the 3D simulation ($w = 0.6\ m$ and $U = 5\ km\ s-1$) liv

List of Tables

Table 1. Methods selected in ANSYS Fluent in CFD simulations 12

Table 2. Mesh Independence test in 2D CFD simulations. 13

Table 3. Dimensionless outflow for 2D simulations with varying window size 25

Table 4. 2D Simulation Results and Ventilation metrics 28

Table 5. Mesh Independence test for the full 3D domain 36

Table 6. Dimensionless out flowrate for 3D cases 39

Table 7. 3D Simulation Results and Ventilation metrics for 3D simulation of the entire 3D domain. .. 41

Table 8. 2D tracer results for an initial concentration of 0.025 li

Table 9. 2D tracer results for an initial concentration of 0.003 lii

Notation and Glossary

A	Cross-section opening area	m^2
A_s	Skin area given by Dubois method	m^2
A_1	Adjusted Model Constant	min^{-1}
b	Distance from the top of the window to the ceiling	m
c	Instantaneous concentration	$mol\ m^{-3}$/ $kg\ m^{-3}$
C	Courant number	
C_d	Discharge coefficient	
C_r	Respiratory coefficient	
$C_{1\varepsilon}, C_{2\varepsilon}, C_{3\varepsilon}$	*k-ε* turbulence models constants	
C_μ, C_v	Turbulent viscosity functions constants	
D	Mass diffusion coefficient	$m^2\ s^{-1}$
E	Empirical constant	
E_p	Human breath out rate of CO_2	$L\ min^{-1}\ person^{-1}$
G_k	Generation of turbulent kinetic energy due to velocity gradients	$kg\ m^{-1}\ s^{-3}$
G_b	Generation of turbulent kinetic energy due to buoyancy	$kg\ m^{-1}\ s^{-3}$
h	Height from the floor	m
h_0	Roughness height	m
h_p	Person height	m
H	Building/Room height	m
H_{3D}	Domain Height	m
l	Opening length	m
L	Length of the building	m
L_{3D}	Domain Length	m
k	Mean Turbulent Kinetic energy per unit mass	$m^2\ s^{-2}$
Ks	Absolute roughness coefficient	m
m_{eq}	Metabolic equivalent	
p	Instantaneous pressure	Pa
P	Pressure	Pa
P_i	Pressure interior	Pa
P_e	Pressure exterior	Pa
Q	Air flow rate	$m^3\ s^{-1}$
Q_O	Flow rate through an orifice	$m^3\ s^{-1}$
Q_{total}	Air flow rate through the window	$m^3\ s^{-1}$
R_ε	RNG additional term for rapidly strained flows	$kg\ m^{-1}\ s^{-3}$
s	Room width	m
s_{ij}	Strain-rate tensor	s^{-1}
S_{ct}	Turbulent Schmidt Number	
S_k, S_ε	Standard *k-ε* user-defined source terms	$kg\ m^{-1}\ s^{-3}$
t	Time	s
TI	Turbulence Intensity	
u_i	Instantaneous velocity in i direction	$m\ s^{-1}$
U	Wind speed	$m\ s^{-1}$
U_{met}	Meteorological wind speed	$m\ s^{-1}$
U_f	Wind frictional speed	$m\ s^{-1}$
V	Volume	m^3
x	Axial coordinate - longitudinal direction	m
x_i	Position vector i direction	m
x_{CO2}	Mass fraction of carbon dioxide	
w	Opening width	m

w_p	Person weight	kg
y	Axial coordinate (altitude)	m
y^*	Y-star	
Y_M	Fluctuation dilatation in compressible turbulence contribution	kg m^{-1} s^{-3}
z	Axial coordinate (Depth)	m
$\%vent$	Ventilation efficiency	
$\%Q_{eff}$	Percentage of effective flowrate	

Greek Letters

$\alpha_k, \alpha_\varepsilon$	Inverse effective Prandtl numbers for k and ε	
β	Thermal expansion coefficient	K^{-1}
ε	Turbulent dissipation rate	m^2 s^{-3}
κ	Von Kármán constant	
μ	Dynamic viscosity	Pa s
ν	Kinematic viscosity	m^2 s^{-1}
$\hat{v}$	Viscosity efficiency	
ρ	Air density	kg m^{-3}
$\sigma_k, \sigma_\varepsilon$	Turbulent Prandtl numbers for k and ε	
τ	Residence time	min
ϕ	Scalar variable	

Indexes

*	Dimensionless variable
$\bar{}$	Mean
$'$	Fluctuating component
^{0}	Initial
eff	Effective
t	Turbulent
$vent$	calculated by tracer simulation data

List of Acronyms

2D	Two Dimensions
3D	Three Dimensions
ABL	Atmospheric Boundary Layer
ACH	Air Change rate per Hour
CFD	Computational Fluid Dynamics
CSTR	Continuous Stirred Tank Reactor
DNS	Direct Numerical Simulation
IAQ	Indoor Air Quality
LES	Large Eddy Simulation
PM	Particle Matter
RANS	Reynolds Average Navier-Stokes
RNG	Renormalization Group
SCE	Sistema de Cerificação Energética e Qualidade do Ar Interior nos Edifícios
VOC	Volatile Organic Compounds

1 Introduction

1.1 Framing and presentation of the work

In the last few decades, the time people spend indoors has increased significantly due to a sedentary lifestyle and work conditions. This has led to an increased studies in understanding this type of environment, namely regarding Indoor Air Quality (IAQ).

IAQ has an enormous impact on our daily lives since it can significantly affect the health, well-being, and comfort of the building's occupants. The indoor air quality is mainly affected by temperature and humidity conditions and the presence of pollutants, such as volatile organic compounds (VOC), nitrogen oxides, ozone, carbon dioxide (CO_2) and other particles, microbiological contaminants, and pathogens. Poor IAQ has been shown to be directly connected with sick building syndrome, reduced productivity, and impaired learning at schools.

This topic attracted much attention in the last two years due to the SARS-CoV-2 pandemic and the need to understand the virus's airborne propagation. It became of fundamental importance to study natural ventilation and how proper ventilation can contribute to a safer environment.

This work focuses on indoor air quality in primary schools, within the scope of the projects 2SMART (https://www.up.pt/2smart/) and SENSINAR (https://sensinair.fe.up.pt/), since it is a context where it has been shown to have associated ventilation problems, with CO_2 concentrations above legislated limits, due to the high number of students per classroom and the long time period of classes.

This dissertation's main focus was the reduction of CO_2 concentration by proper natural ventilation in classrooms. This was studied using Computational Fluid Dynamics (CFD) in order to test different room designs and assess IAQ, namely if the CO_2 legislated limits were or not reached. Design parameters were studied for the optimization of wind-driven ventilation of a classroom, for example, the volume of the room, the window dimensions and the atmospheric conditions, i.e. the wind speed.

This work consists in preliminary studies of the natural ventilation in a real classroom from a school in the metropolitan area of Porto, Portugal. These preliminary studies only consider one window and any classroom objects, such as desk, chairs, cupboard are not considered.

1.2 Contribution of the author to the work

All the work presented in this dissertation, namely the CFD simulations and respective building of geometry and mesh, was done by the author, with the guidance of the supervisor Margarida Brito and co-supervisor, Sofia Sousa. Professor Ricardo Santos also contributed to this works with his guidance and expertise on CFD. Mateus Caixeta helped and guided during the construction of the 3D meshes.

1.3 Organization of the dissertation

This dissertation is divided into 6 chapters:

The first chapter, Chapter 1, briefly introduces the framing and context of this work and the studies developed.

Chapter 2 is a review of the current knowledge of the scientific community in natural ventilation, more specifically, in the simulation of this phenomena using CFD. In this section, the most important results and recommendations reported by other researchers are presented.

In Chapter 3, a first 2D CFD approach to the problem is assessed. In this section, the numerical methods are validated, and the effect of some of the simulation parameters, such as the window dimensions and the wind speed, is explored. The first insights on ventilation efficiency are also presented.

Chapter 4 describes the work done with a 3D model: validation of the model, flow structure of the case and the effect of some parameter on ventilation are again explored. In this section, the comparison between the 2D and 3D model is investigated.

Conclusions of this dissertation are presented in Chapter 5, and the assessment of the work done, and future work suggestions are discussed in Chapter 6.

2 Context and State of the art

Indoor Air Quality has been a concern among many modern communities due to the long time people spend indoors. Studies suggest that people spend around 80 % to 90 % of their lifetime indoors on average (Megahed and Ghoneim (2021)). In the last two years, due to the SARS-CoV-2 pandemic, indoor ventilation has become a topic of even greater importance since proper ventilation is fundamental to ensure a safer environment (Fadaei (2021)). Furthermore, air ventilation is also crucial to improve thermal comfort in the warmer seasons and control humidity in moderate humid climates.

In Portugal, the national system of energy certification and indoor air quality in buildings (SCE) has the main goal of regulating energetic efficiency and IAQ conditions. For the specific case of classrooms, which is the main topic of this work, in the regulation n. º 138-G/2021 of 1st of July (Ministérios do Ambiente 2021), some of the requirements for IAQ are specified, such as, the minimal flow rate of fresh air for a typical classroom, $24\ \mathrm{m^3\ hour^{-1}\ person^{-1}}$, or the protection limit for the most problematic classroom pollutants, e.g., particulate matter (PM), CO_2 and VOC.

The present work focuses on the reduction of CO_2 concentration by proper natural ventilation in classrooms. As mentioned before, the protection limit for carbon dioxide concentration is legislated and it is defined as $2250\ \mathrm{mg\ m^{-3}}$ (with a tolerance for 30 % for new and existing buildings, including renovated ones, without mechanical ventilation systems)

The human exhale rate of CO_2, E_p, has been widely studied (Batterman 2017) and for a primary classroom with 25 children aged 6 to 10 years old, the breathed-out CO_2 rate is roughly $5\ \mathrm{L\ min^{-1}}$. This means that in a class of 2 hours, the breathed-out concentration of CO_2 is approximately $8\ \mathrm{g\ m^{-3}}$, which is four times higher than the value given as the limit by SCE, and this is considering only the CO_2 emitted by the children and does not take into account other possible sources. Moreover, some studies have reported that increasing ventilation rates in classrooms and decreasing CO2 concentrations positively affect children's short-term concentration and logical thinking (Petersen et al. 2016). This evidences the importance of proper ventilation in classrooms.

Most school buildings are conditioned with one of three types of ventilation: natural ventilation, mixing ventilation and displacement ventilation. However, in Portugal, in the context of classrooms, natural ventilation is by far the most relied upon.

2.1 Natural Ventilation

Natural ventilation is a system of ventilation that supplies fresh air to an indoor space, removing the aged air. This is done without mechanical devices, and only based on pressure differences, mainly due to wind, and temperature differences (wind-driven and buoyancy-driven ventilation) (Weerasuriya et al. 2019).

The interest in natural ventilation stems from the possibility of energy saving when implemented in buildings designs, which also implies a more environmentally friendly construction (Yik and Yu Fat 2010, Oropeza-Perez and Østergaard 2014, Weerasuriya et al. 2019). For example, Yik and Yu Fat (2010) studied the possibility of saving energy by integrating natural ventilation in public houses in Hong Kong since, for most days, natural ventilation was enough to ensure thermal comfort. It has been reported that the energy cost in naturally ventilated buildings is 40 % less than in buildings using mechanical ventilation, such as air conditioning (CIBSE 2000).

The main issue related to the natural ventilation in buildings is the difficulty to control and predict because it will heavily depend on a plethora of factors, namely, wind direction and speed, atmospheric pressure, temperature and humidity conditions, geometry, dimensions and position of the building itself, normal activity inside the building, among others. Another disadvantage of natural ventilation is the humidity of the fresh air, which makes this system less attractive in very humid climates.

The efficiency of natural ventilation can be quantified by

$$ACH = \frac{Q}{V} \qquad (1)$$

where V is the indoor volume and Q the air flow rate (Chu et al. 2015).

The experimental estimation of Q in Equation (1) is not an easy task. Considering Bernoulli's hypothesis of incompressible and inviscid flow, the orifice equation could be used to calculate steady flow rate of wind-driven ventilation from

$$Q_O = C_d A \left(\frac{2|P_e - P_i|}{\rho} \right)^{1/2} \qquad (2)$$

where A is the cross-section opening, C_d the dimensionless discharge coefficient, ρ the air density and P_e and P_i the external and internal pressures. However, several studies, such as Fordham (2000) and Warren (1977), have shown that this equation does not predict the flow in buildings since the time average pressure difference is close to zero.

During the last two decades, the efficiency of natural ventilation has been widely studied using experimental techniques, such as tracer gas (Kato et al. 2006, Ji et al. 2011), wind tunnels with reduced and full-scale models (Larsen and Heiselberg 2008, Kato et al. 2006), and CFD models (Zhang, Weerasuriya, and Tse 2020, Blocken, Stathopoulos, and Carmeliet 2007, Zhuang, Li, and Tu 2014).

Many researchers have tried to develop empirical and semi-empirical models to predict air exchange rate. For example, Warren (1977) proposed an expression to predict the exchange rate with a single windward opening of a building,

$$Q^* = \frac{Q}{UA} = [0.022\,, 0.026] \qquad (3)$$

where Q^* is the dimensionless exchange rate and U the wind speed. However, this empirical value range was obtained for only a restricted range of windows: square windows with an area between $0.016 - 0.065\ \mathrm{m}^2$ and slot windows with a range of $0.127 - 0.203\ \mathrm{m}^2$. These types of windows are not common in the context of classrooms since those windows tend to have larger dimensions.

Warren and Parkins (2013) concluded that wind and buoyancy driven ventilation are significantly different, and their contributions should be estimated separately. Cockroft and Robertson (1976) also reported that only 37 % of the airflow contributed for the effective ventilation of the room. This was estimated by ACH using a tracer gas decay method and validated from measurements using velocity sensors. Nevertheless, Larsen and Heiselberg (2008) also performed the same study and reported that the deviation between the two methods was only 10 to 20 %.

2.2 Computational Fluid Dynamics in Natural Ventilation Studies

Computational Fluid Dynamics (CFD) has become an essential tool for natural ventilation investigation since it does not require any actual real models (full-scale or not), costly installations like wind tunnels or actual products like tracer gases. Therefore, it is a very flexible tool when compared with others. Moreover, CFD simulations produce more data when compared to other methods.

CFD is the branch of fluid dynamics that simulates fluid motion and heat transfer using numerical approaches. CFD methods consist in solving the differential equations of mass, energy, and momentum, also known as the Navier-Stokes equations, in order to predict the behaviour and characteristics of fluid flow.

For three-dimensional, incompressible viscous flow, these equations are the continuity equation given by

$$\frac{\partial u_i}{\partial x_i} = 0 \qquad (4)$$

and the Navier-Stokes equations, given by

$$\frac{\partial u_i}{\partial t} + \frac{\partial}{\partial x_j}\left(u_i u_j\right) = -\frac{1}{\rho}\frac{\partial p}{\partial x_i} + \frac{\partial}{\partial x_j}\left(2\nu s_{ij}\right) \qquad (5)$$

where u_i is the velocity vector, and p the pressure.

In the case of building ventilation, more specifically wind-driven ventilation, the domain is usually the atmospheric boundary layer (ABL), which is defined as the lower region of the troposphere, with an altitude between 0 and 200 m. ABL is a turbulent boundary layer where, in the context of flow in urban areas, the variation of the fluid's properties can usually be neglected (Franke et al. 2004).

Turbulent flows are characterized by fluctuating velocity fields, that mix transported quantities such as momentum, energy, and concentration (ANSYS 2022). In order to describe these types of flows, the Navier-Stokes can be solved on very fine meshes, which are able to capture all the relevant scales of the flow, and with long enough time-dependent solutions to yield a stable time average solution. This direct method is called Direct Numerical Simulation (DNS) and is normally not used since it is very computationally intensive. Therefore, the general method used for turbulent flow computing flow is the Reynolds Average Navier-Stokes (RANS) approach, where the equations are averaged in time for all turbulent scales in order to yield statistically steady solutions (Franke et al. 2004). These will lead to the additional terms in the momentum equation, which represent the effect of turbulent fluctuations on the average flow. These new terms are called the Reynolds stresses that can be modelled using different models, the turbulence models. These models consist of decomposing the Navier-Stokes equations into mean and fluctuating components, as generally described by

$$u_i = \bar{u}_i + u_i' \qquad (6)$$

$$\phi = \bar{\phi} + \phi' \qquad (7)$$

where equations (6) and (7) are the decomposition for the velocity components, and the other scalar quantities such as pressure, energy, or species (denoted as ϕ), respectively.

Another approach often used for these types of problems is Large Eddy Simulation (LES), where the large, energy-containing eddies are simulated accurately on a fine mesh and the effects of the smaller, dissipate eddies are resolved using a subgrid-scale stress model. LES uses a series

of filtering equations that manipulate the Navier-Stokes equation to remove eddies smaller than the size of the filter.

2.2.1 Turbulence models

There are a plethora of turbulence models, that differ in origin and approach to the problem. For the context of this work, only the Standard *k-ε* model and its derivates are discussed, since they are well implemented in the software used, commercial package ANSYS Fluent, and are normally employed in natural ventilation studies.

2.2.1.1 Standard *k-ε* Model

Standard *k-ε* Model, which was first proposed by Launder (1972), is widely used due to its robustness, economy, and reasonable accuracy in a wide range of turbulent flows. It is a semi-empirical model based on transport equations for the turbulent kinetic energy, k, and for the turbulent dissipation rate, ε, given by

$$\frac{\partial}{\partial t}(\rho k) + \frac{\partial}{\partial x_i}(\rho k u_i) = \frac{\partial}{\partial x_j}\left[\left(\mu + \frac{\mu_t}{\sigma_k}\right)\frac{\partial k}{\partial x_j}\right] + G_k + G_b - \rho\varepsilon - Y_M + S_k \qquad (8)$$

$$\frac{\partial}{\partial t}(\rho \varepsilon) + \frac{\partial}{\partial x_i}(\rho \varepsilon u_i) = \frac{\partial}{\partial x_j}\left[\left(\mu + \frac{\mu_t}{\sigma_\varepsilon}\right)\frac{\partial \varepsilon}{\partial x_j}\right] + C_{1\varepsilon}\frac{\varepsilon}{k}(G_k + C_{3\varepsilon}G_b) - C_{2\varepsilon}\rho\frac{\varepsilon^2}{k} + S_\varepsilon \qquad (9)$$

These equations are derived from the exact equations assuming a fully turbulent flow and negligible molecular viscosity effects. In these equations, G_k accounts for the generation of k due to mean velocity gradients and G_b for the generation of turbulent kinetic energy due to buoyancy. Y_M represents the contribution of the fluctuating dilatation in compressible turbulence to the overall dissipation rate. S_k and S_ε are user-defined source terms. The turbulent viscosity, μ_t, is given by

$$\mu_t = \rho C_\mu \frac{k^2}{\varepsilon} \qquad (10)$$

where C_μ is a constant.

In Equations (8) and (9), $C_{1\varepsilon}$, $C_{2\varepsilon}$, and $C_{3\varepsilon}$ are constants, and σ_k and σ_ε are the turbulent Prandtl numbers for k and ε, respectively. The values for the model constants are $C_{1\varepsilon} = 1.44, C_{2\varepsilon} = 1.92, C_\mu = 0.09, \sigma_k = 1.0$ and $\sigma_k = 1.3$, which were derived from experiment for fundamental turbulent flows.

2.2.1.2 RNG *k-ε* Model

This model is one of the variations of the Standard *k-ε* model, and the main difference is its derivation. RNG model was derived using a statistical technique called renormalization group theory (RNG). It is similar in form to the standard model, but it has an additional term in its

equation for the turbulent dissipation rate, which includes the effect of swirl on turbulence and provides an analytical expression for turbulent Prandtl numbers and a differential expression for effective viscosity that accounts for low Reynolds number effects. These features make RNG *k-ε* model more accurate and reliable for a wider class of flows than Standard model. The transport equations in RNG *k-ε* model are given by

$$\frac{\partial}{\partial t}(\rho k) + \frac{\partial}{\partial x_i}(\rho k u_i) = \frac{\partial}{\partial x_j}\left[\alpha_\kappa \mu_{eff}\frac{\partial k}{\partial x_j}\right] + G_k + G_b - \rho_\varepsilon - Y_M + S_k \quad (11)$$

$$\frac{\partial}{\partial t}(\rho \varepsilon) + \frac{\partial}{\partial x_i}(\rho \varepsilon u_i) = \frac{\partial}{\partial x_j}\left[\alpha_\kappa \mu_{eff}\frac{\partial \varepsilon}{\partial x_j}\right] + C_{1\varepsilon}\frac{\varepsilon}{k}(G_k + C_{3\varepsilon}G_b) - C_{2\varepsilon}\rho\frac{\varepsilon^2}{k} - R_\varepsilon + S_\varepsilon \quad (12)$$

In the RNG model, the turbulence viscosity is obtained by integrating equation given by

$$d\left(\frac{\rho^2 k}{\sqrt{\varepsilon\mu}}\right) = 1.72\frac{\hat{v}}{\sqrt{\hat{v}^3 - 1 + C_v}}d\hat{v} \quad (13)$$

where $\hat{v}$, is

$$\hat{v} = \frac{\mu_{eff}}{\mu} \quad (14)$$

For high Reynolds number, the solution becomes the equation used in Standard model, with $C_\mu = 0.0845$, which is similar to the empirical determined value for the standard model. In Ansys FLUENT package, the high Reynolds solution is used, but there is the option to include low Reynolds number effects.

2.2.1.3 Realizable *k-ε* model

Realizable *k-ε* model addresses some shortcomings of the traditional *k-ε* models. It adopts a turbulent viscosity expression with a variable C_μ, first proposed by Reynolds (1987), and a new equation for ε based on the dynamic equation mean-square vorticity fluctuation. The transport equations for the realizable *k-ε* model are

$$\frac{\partial}{\partial t}(\rho k) + \frac{\partial}{\partial x_i}(\rho k u_i) = \frac{\partial}{\partial x_j}\left[\left(\mu + \frac{\mu_t}{\sigma_k}\right)\frac{\partial k}{\partial x_j}\right] + G_k + G_b - \rho\varepsilon - Y_M + S_k \quad (15)$$

$$\frac{\partial}{\partial t}(\rho \varepsilon) + \frac{\partial}{\partial x_j}(\rho \varepsilon u_j) = \frac{\partial}{\partial x_j}\left[\left(\mu + \frac{\mu_t}{\sigma_\varepsilon}\right)\frac{\partial \varepsilon}{\partial x_j}\right] + \rho C_1 S\varepsilon - \rho C_2\frac{\varepsilon^2}{k + \sqrt{v\varepsilon}} + C_{1\varepsilon}\frac{\varepsilon}{k}C_{3\varepsilon}G_b + S_\varepsilon \quad (16)$$

The transport equation for k is the same than in the standard model. The turbulent viscosity, μ_t, is given by Equation (10), but unlike the other methods, C_μ is no longer constant but expressed by a function of the mean strain and rotation rates, the angular velocity of the system rotation, and the turbulence fields (ANSYS 2022).

2.2.2 Natural Ventilation CFD Simulations

Several studies have been made on natural ventilation either using CFD or experimental techniques (Zhang, Weerasuriya, and Tse 2020, Evola and Popov 2006, Franke et al. 2004). Most propose the RNG *k-ε* model as the most indicated for natural ventilation since it seems to produce fairly consistent results. However, this model is still quite computational time consuming. The other method widely implemented is LES, but this method is even more computational time consuming, and it is only recommended when extreme precision is required (Evola and Popov 2006).

In CFD simulations, it is very crucial to define a proper domain. In wind engineering problems, this presents an additional challenge, namely, how big and detailed the domain should be in order to produce reliable results. Two approaches are usually used: coupled or decoupled approaches. In the couple approach, both the building and the environment around it are modelled at the same time, enabling the simulation of the indoor and outdoor air flows. In the decoupled approach, the two parts are modelled separately by using the wind pressure at the surface of the building, obtained with the atmosphere domain simulation, as input for the indoor simulation. The decoupled approach has a clear advantage of being less computationally intensive. However, it presents many drawbacks in terms of accuracy, and it is clear that the coupled approach is preferred.

Regarding the size of the domain, Hall (1997) and Baetke, Werner, and Wengle (1990) proposed some guidelines. The authors reported that the inlet should be at least $5H$ away from the building, where H is the height of the building, and the outflow boundary at least at $15H$, to enable for flow development. The minimum height of the computation domain has been shown as $5H$, in order to prevent artificial acceleration at the top of the building. In 3D simulations, the lateral extension should be enough to produce a blockage ratio, which is usually defined as the projected area of the structure in flow direction to the cross-sectional area of the domain around the structure, of less than 3 %.

Regarding the detail required for reliable simulations, most researchers report that it will heavily depend on the application. Nevertheless, some considerations seem to be universal: the level of detail for individual buildings will depend on the distance to the building of interest, and so, a simple block structure is enough for further away buildings but for the central building, features greater than 1 m should be represented.

Another crucial design point to consider is the boundary conditions that represent the influence of the surroundings of the computational domain. In the literature, most researchers seem to agree that symmetry condition is indicated both for the top and lateral boundaries (Franke et al. 2004). However, some studies report that considering these boundaries as the outflow is

also interesting since it considers the natural outflow due to the increasing displacement of the fluid. For the inlet, some authors use a logarithmic wind profile with wind tunnel experiments data (Zhang, Weerasuriya, and Tse 2020, Evola and Popov 2006),

$$U(h) = \frac{U_f}{\kappa} \ln\left(\frac{h}{h_0}\right) \quad (17)$$

while others Allocca, Chen, and Glicksman (2003) use a profile for local wind based on meteorological wind speeds, U_{met}, usually referred as the power profile,

$$U\,(h) = 0.35 U_{\text{met}} h^{0.25} \quad (18)$$

with 0.25 the constant used for atmospheric flow.

Some researchers assume a constant wind front if the height of the domain is not very large.

Another important factor that has been studied in the context of CFD simulation for building ventilation analysis concerns important considerations in ABL flow simulation, namely the accuracy of the description of the flow near the ground surface. Blocken, Stathopoulos, and Carmeliet (2007) proposed some requirements to achieve this: having a sufficiently fine mesh near the walls; ensuring a horizontally homogeneous flow in the upstream and downstream region; considering the influence of the physical roughness of the walls and its relationship with aerodynamic roughness length.

As aforementioned, most existing studies focus on characterizing the influence of one or a group of parameters in a specific configuration. Chu and Chiang (2014) studied the effect of the ratio between building length and ceiling height in natural cross ventilation using LES simulations and reported that it should be less than five to increase effective ventilation. Other authors, Zhuang, Li, and Tu (2014), used RANS and LES to study the effect of the wind incident angle and found out, that for natural single sided ventilation, the effective ventilation rate would steadily decrease as the angle formed with the windward side varies between 0º (windward side) to 90º, but it would increase for leeward side ventilation (180º).

Another interesting study was performed by Chu et al. (2015) to quantify the air exchange rate in a natural ventilated building with more than one opening in the same wall, a configuration much present in classrooms and reported, using the tracer gas decay method, that the *ACH* was linearly correlated with the wind speed and opening area. The same conclusion was reached by Wang and Chen (2012) using LES model.

Within the scope of this work, the natural ventilation of a primary classroom was simulated taking into account all the considerations made by the authors mentioned in this section, namely domain size, turbulence models, boundary conditions, among others.

3 2D Simulation of Natural Ventilation

As a first approach, a simplified 2D case was considered. Two configurations of a single room were studied: single-sided ventilation that consists of a window on the windward side and cross-ventilated with two opposite windows. To validate the numerical methods, the effect of wall rugosity, turbulence model, turbulence intensity at the inlet and of the mesh were studied.

3.1 Numerical Methods Validation

3.1.1 Computation Domain and Solution Methodology

The simulation domain consists of a single room with one or two openings surrounded by an atmosphere around the building. Figure 1 shows the 2D CFD domain simulated. According to the literature, this approach of simulating both the indoor and the outdoor is the one that achieves the most reliable results. Both windows have the same size and are at the same distance from the ground. As recommended in the literature, the representation of the atmosphere depends on the dimensions of the room, i.e., the height, H (Figure 1). For this case, $L = H = 3$ m and $w = 0.6$ m.

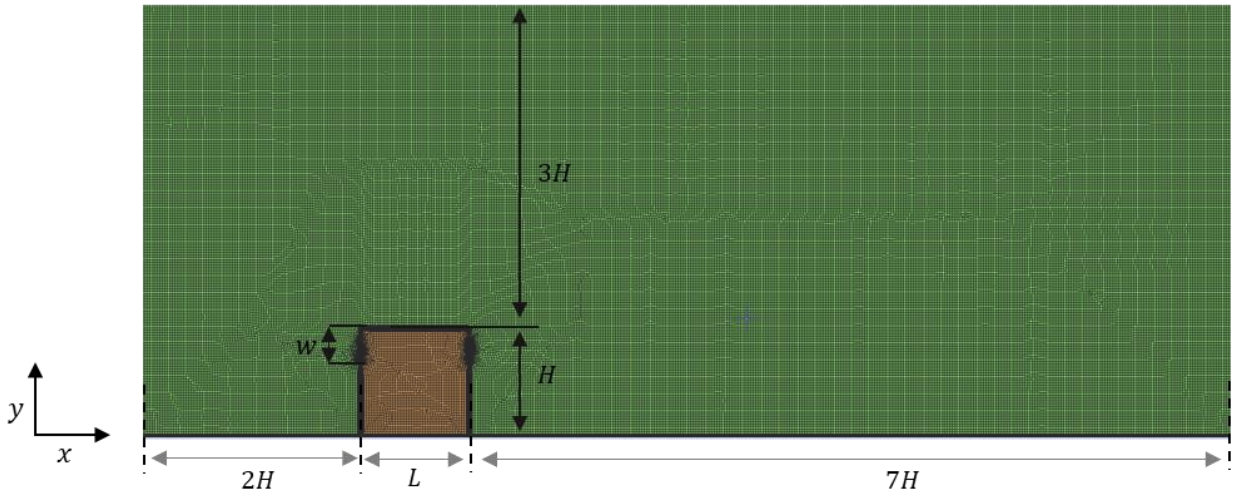


Figure 1. Geometry and mesh of the 2D domain.

The left, right, top, and bottom boundaries were defined as inlet, outlet, symmetry, and wall, respectively, the rest of the domain was set as fluid. The mesh was the same for both indoor and outdoor, with an element size of 0.067 m. For every wall surface, inflation with 10 maximum layers and a growth rate of 1.2 was applied. An edge sizing was implemented at the windows.

For the simulation, the gravity was enabled, the air density and viscosity were constant at $1.225\ \mathrm{kg\,m^{-3}}$ and $1.7 \times 10^{-5}\ \mathrm{Pa\,s}$, respectively, and the flow was considered isothermal.

To model the turbulence, the standard k-ε model with standard wall functions was used. The standard wall functions are described by

$$U^* = \frac{1}{\kappa} \ln (E y^*)$$

where U^* is the dimensionless velocity and y^* the dimensionless distance from the wall.

A constant wind speed of $5\ \mathrm{km\ h^{-1}}$ was considered at the inlet. For the turbulence input, 4% of turbulence intensity and $0.4\ \mathrm{m}$ of turbulence length were used, according to the values reported in the literature (Zhang, Weerasuriya, and Tse 2020, Evola and Popov 2006, Jiang et al. 2003). The windward side window was defined as interior; and the leeward side opening was defined as a wall for single sided ventilation and as interior for cross ventilation. Table 1 shows the methods used. The simulation was initialised using hybrid initialisation and the convergence criteria were residuals lower than 10^{-6}.

The flow was simulated using the Finite Volume software package ANSYS/Fluent 2021.

Table 1. Methods selected in ANSYS Fluent in CFD simulations

Methods	
Pressure-Velocity Coupling	
Scheme	Coupled
Flux type	Rhie-Chow
Spatial Discretisation	
Gradient	Least Squares Cell Based
Pressure	Second Order
Momentum	Second Order Upwind
Turbulent kinetic Energy	Second Order Upwind
Turbulent Dissipation Rate	Second Order Upwind
Pseudo-Transient	Enable

3.1.2 Mesh Independence Test

A mesh independence test was done using three meshes with different numbers of elements. The meshes name refer to the number of elements, in millions. In Mesh 2D_0.09M, the element size at the windows was 0.005 m, and it has 95 081 cells, as shown in Figure 1. Meshes 2D_0.06M and 2D_0.1M have 68 975 cells and 160 778 cells.

The mesh independence study consisted of the simulation of flow at single sided ventilation and the comparison was based on the average x-velocity at the windward opening of the building, $\bar{u}_{windward}$, for the three meshes. Table 2 shows the CFD results of the average x-velocity. The value obtained with the last two meshes was less than 0.1 % of variation, and thus Mesh
2D_0.09M was considered valid.

Table 2. Mesh Independence test in 2D CFD simulations.

Mesh	Elements	$\bar{u}_{windward}$ $(\mathrm{m\ s^{-1}})$
2D_0.06M	68 975	7.8×10^{-3}
2D_0.09M	95 081	5.60×10^{-3}
2D_0.1M	160 778	5.58×10^{-3}

3.1.3 Single Sided Ventilation

To understand the influence of some simulation designs, parameters and domain characteristics, several studies of single sided ventilation were performed. The base case considered for these studies was the single-sided ventilation case described in Section 3.1.1

Figure 2 shows the plot of x-velocity at the window.

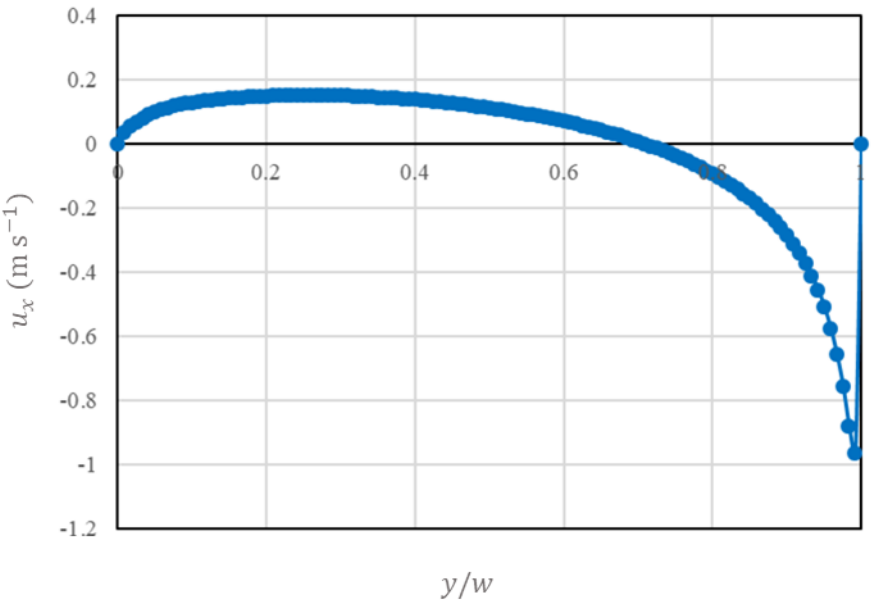


Figure 2. x-velocity profile at the window for single sided ventilation determined from 2D CFD model.

It shows that approximately 70% of the window edge corresponds to the air inlet, and 30% is the outlet of the room. The air leaves mainly in the very top part of the window, as a jet.

Figure 3 shows the streamlines obtained in the simulation of single sided ventilation. Results show that the flow goes mostly over the building, while ate the interior of the building, the streamlines form close circulation loops. These flow patterns make the ventilation of the room not very efficient. The same conclusions can be drawn from Figure 4, which shows the velocity vectors in the room. The velocity vector highlighted the fact that the flow dynamics in the room is only a fraction of the one in the outside

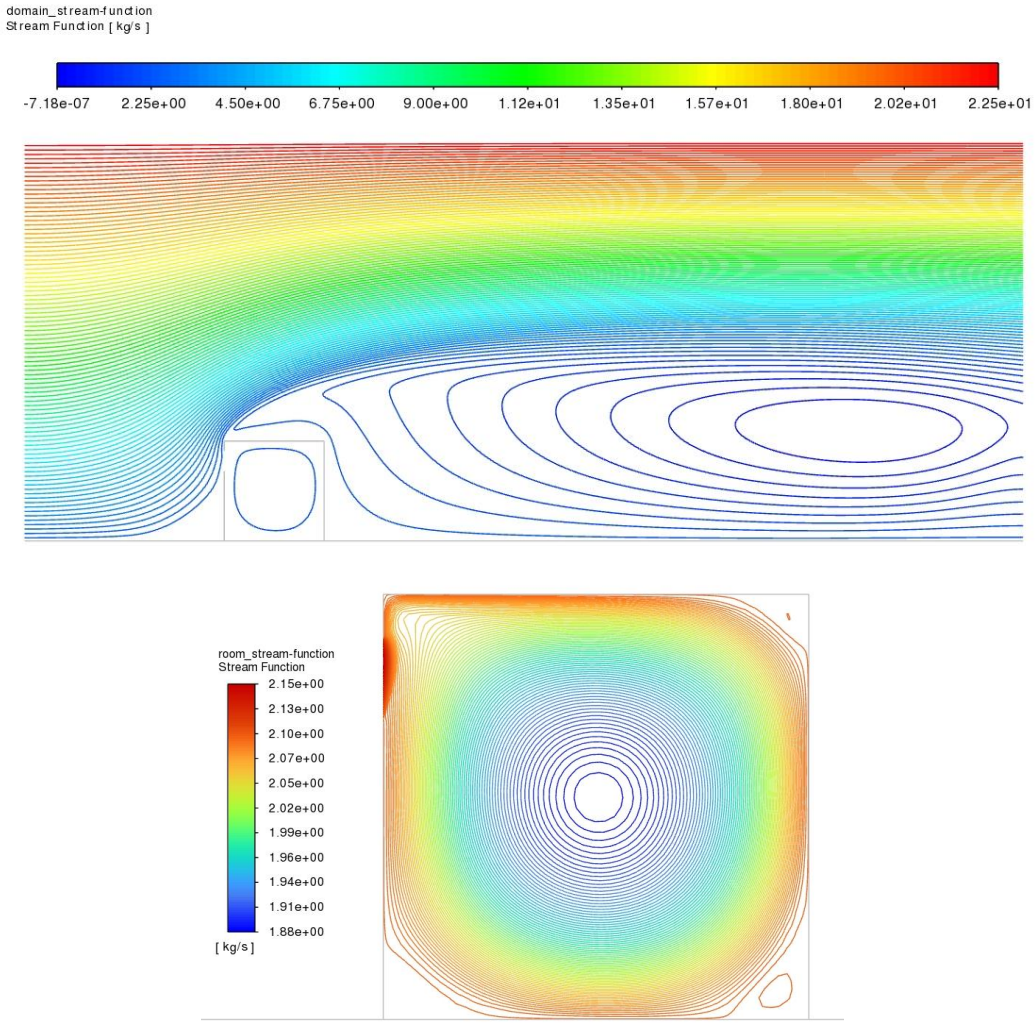


Figure 3. Streamlines for single sided ventilation: full domain (top); indoor (bottom) determined from 2D CFD simulations

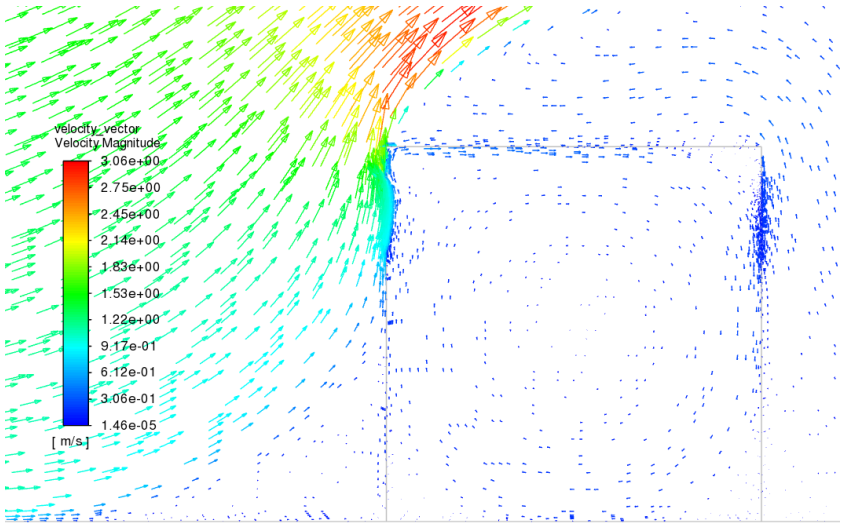


Figure 4. Velocity vector field for single sided ventilation determined from 2D CFD simulations

3.1.3.1 Wall Roughness effect

The influence of the wall roughness in the converged solution was also studied in this work for the single sided ventilation simulation using the standard k-ε model. It was considered a roughness coefficient of 0.5 and a roughness height, Ks, equal to the absolute roughness coefficient that, for smooth cement, ranges from 3×10^{-4} to 1×10^{-3}m. Figure 5 shows the velocity profiles at the window for Ks values of $0, 2 \times 10^{-4}, 3 \times 10^{-4}, 6 \times 10^{-4}$ and 1×10^{-3} m.

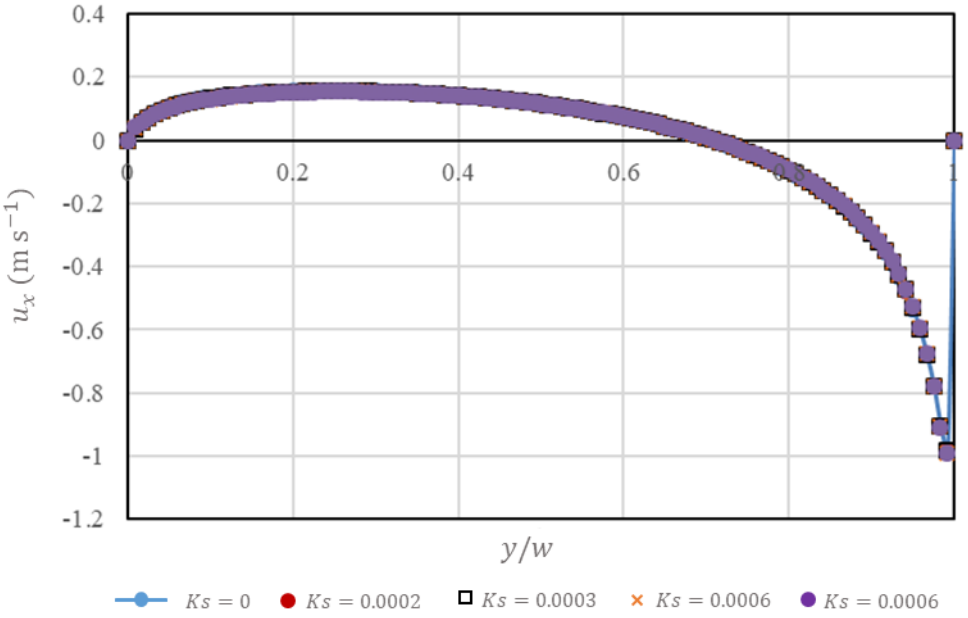


Figure 5. x-velocity profiles determined from 2D CFD simulations for different Ks, using standard k-ε. $Ks = 0\ m$ (blue); $Ks = 2 \times 10^{-4}\ m$ (red); $Ks = 3 \times 10^{-4}\ m$ (squares); $Ks = 6 \times 10^{-4}\ m$ (crosses); $Ks = 1 \times 10^{-3}\ m$ (purple).

It is clear that Ks has no influence on the x-velocity profile at the window. The value of the wall roughness did not change the computational time of the simulation, in future simulations, a value of Ks of 6×10^{-4} m was used.

3.1.3.2 Influence of Turbulence Models

The influence of other turbulence models was also studied in this work, namely, Realisable k-ε, RNG and LES. These results were compared to CFD simulations using standard k-ε, in Section 3.1.3.

The Realisable k-ε and RNG models, which are versions of the 2-equation k-ε to model turbulence, were set to simulate steady-state simulations.

LES was set in dynamic simulation. The simulation was run for 4950 time-steps of 0.0036 s each. The time step was defined for a Courant number, $C = \frac{u\Delta t}{\Delta x}$, of 1 considering the element at the window and the air velocity at the inlet.

Figure 6 compares the velocity profiles obtained for the four turbulent models. The velocity profile obtained foe LES was time averaged over the 4950 time-steps of the dynamic simulation. Results show that the profiles are almost identical and the standard k-ε only shows a slight difference in the magnitude of minimum velocity at the outlet jet.

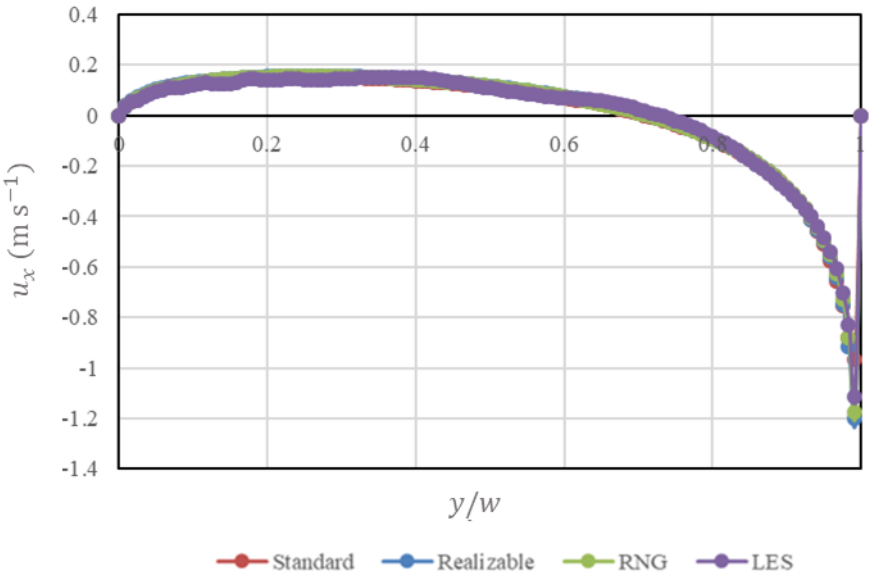


Figure 6. x-velocity at the window for single sided ventilation using 2D CFD model and Standard k-ε (red); Realisable k-ε (blue); RNG (green); LES (purple).

3.1.3.3 Effect of the Inlet Turbulence Intensity

Another factor that seemed interesting to analyse was the inlet turbulence conditions, more specifically the turbulence intensity, TI. As described in Section 3.1.1 simulations were run using $TI = 4\ \%$ according to previous works and experimental data in the literature (Evola and Popov 2006, Zhang, Weerasuriya, and Tse 2020). The single sided ventilation case was simulated for TI values of 1 %, 4 % and 10 %. Figure 7 shows the x-velocity profile for the three cases. Results show that there is no significant change in the velocity profile at the window. Therefore, in further simulations, the turbulent intensity was set as 4 %.

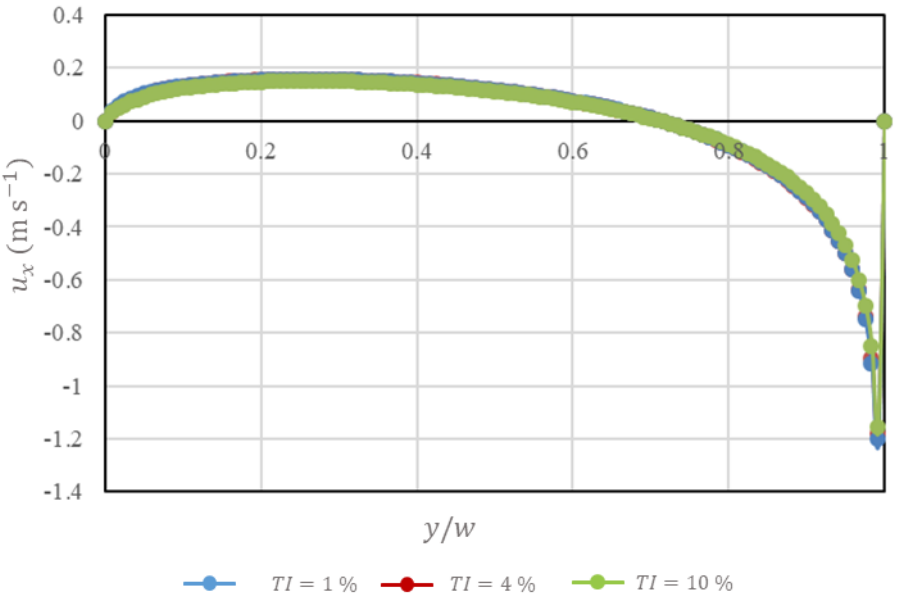


Figure 7. x-velocity profile at the window for $TI = 1\ \%$ (red), $TI = 4\ \%$ (blue) and $TI = 10\ \%$ (green) determined from 2D CFD model.

3.1.4 Cross Ventilation

As mentioned before, cross ventilation was also studied. Figure 8 and Figure 9 show the streamlines and velocity vectors using Mesh 1 and the standard k-ε model, $TI = 4\ \%$ and $K_s = 0.0006\ \mathrm{m}$. In this simulation, the air enters at the windward side window and leaves by the leeward side, which promotes the air flow inside the room. By analysing the x-velocity profiles in Figure 10, the air flow is also clearly observed. It is also interesting to note that the velocity profiles have different shape. For the windward side window, the lower part of the window appears to have a parabolic profile while the top profiles seem more linear. For the leeward side the opposite can be noticed from Figure 10.

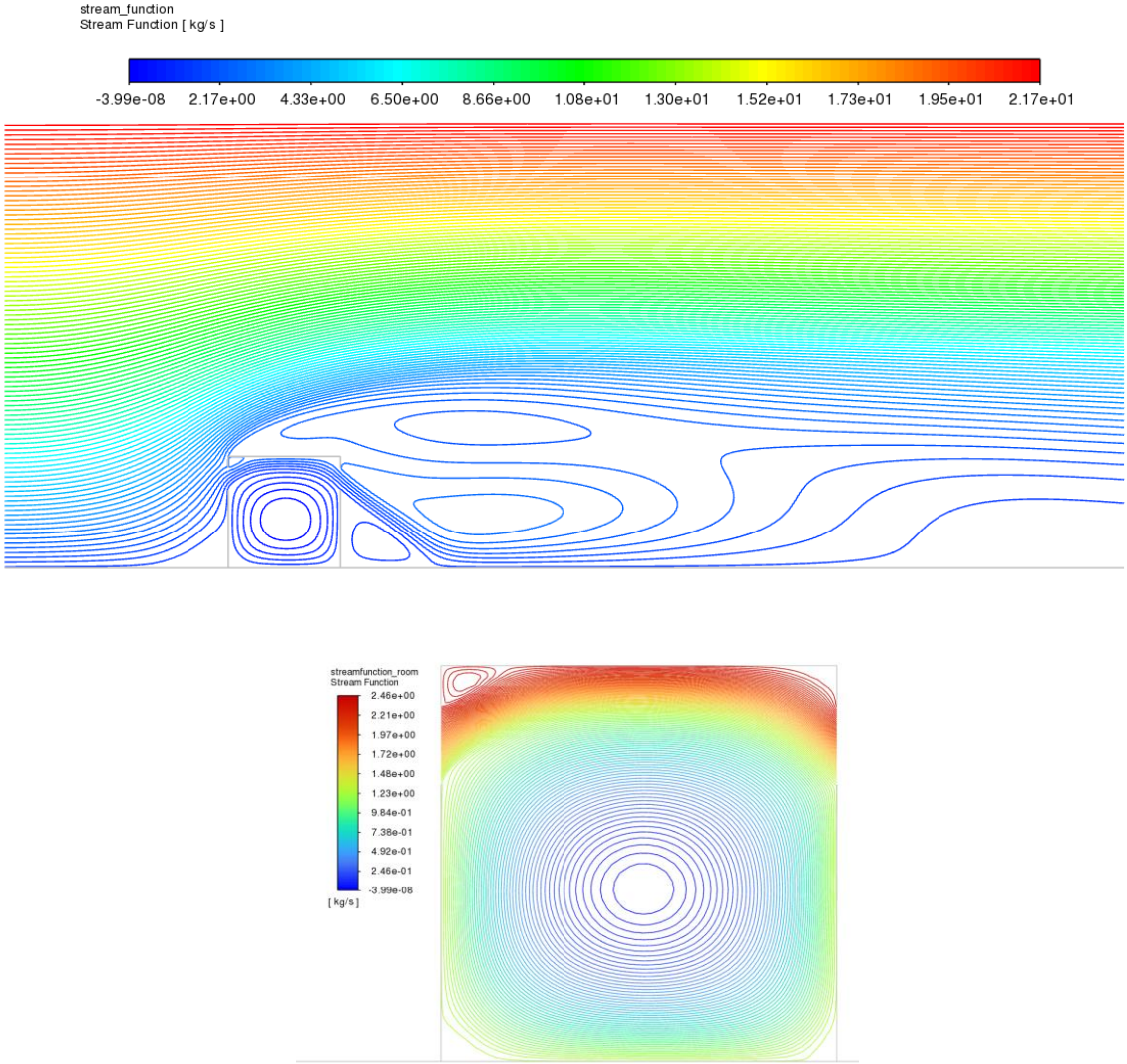


Figure 8. Streamlines for cross ventilation: full domain (top); indoor (bottom) in 2D CFD simulations.

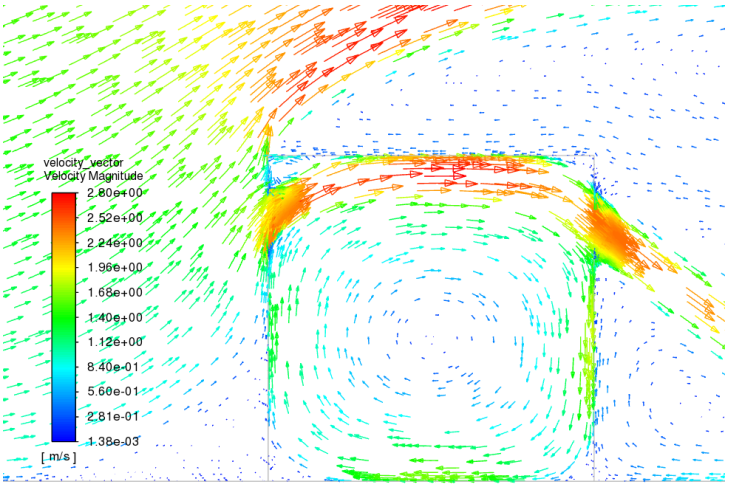


Figure 9. Velocity vector field for cross ventilation using 2D CFD simulations.

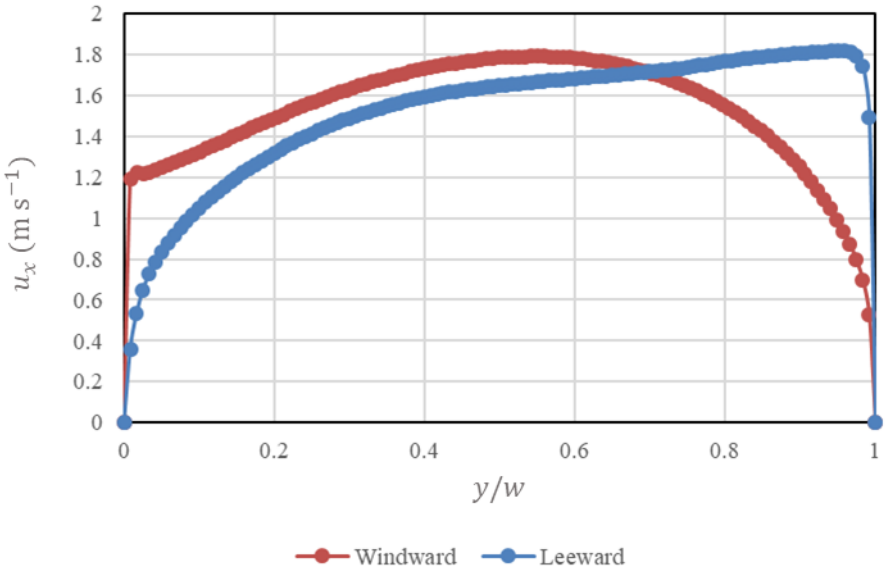


Figure 10. x-velocity profile at the window for single sided ventilation: Windward side (blue); Leeward side (red).

3.2 Ventilation Parameter Study

Another study was performed in order to analyse the effect of some parameters on the ventilation rate, namely, the wind speed, U, the window size, w, the room height and length, H and L, and the window position, b, as shown in Figure 11.

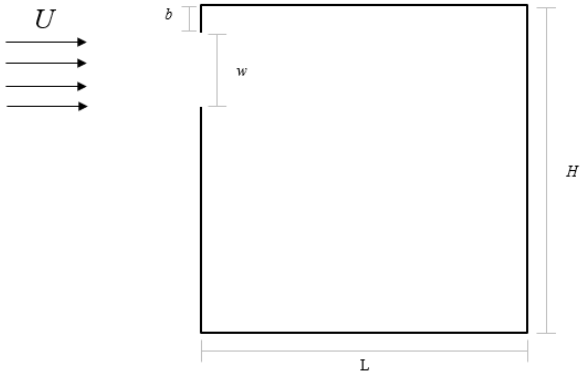


Figure 11. Sketch of the window and the geometric parameters and wind speed studied in 2D CFD simulation.

3.2.1 Effect of Wind Speed

The ventilation of a room by wind driven natural ventilation is dependent on the wind speed near the opening. To access this effect, the wind speed, U, was studied. According to GMAO (2022), the average wind velocity is approximately $11.6\ \mathrm{km\ h^{-1}}$, in the windier season in Porto, December and January. In the less windy season, the velocity is roughly $9\ \mathrm{km\ h^{-1}}$.

Three new cases were simulated according to the setup described in Section 3.1, using the RNG turbulence model and changing the inlet wind speed to $U = 9\ \mathrm{km\ h^{-1}}$, $10\ \mathrm{km\ h^{-1}}$ and $11.6\ \mathrm{km\ h^{-1}}$. Figure 12 shows the x-velocity profile at the window for all 4 wind speeds simulated. Analysing this figure, the magnitude of x-velocity increases with the wind velocity, resulting in a higher ventilation rate. However, it is also possible to conclude that the shape of the velocity profile, that is that the top 30% of the window serves as an outlet while the other 70% function has an inlet, is independent of the wind speed. This is quite evident if the normalised x-velocity profiles are plotted, $u_x^* = \frac{u_x}{U}$. Figure 13 shows the normalized profiles of u_x.

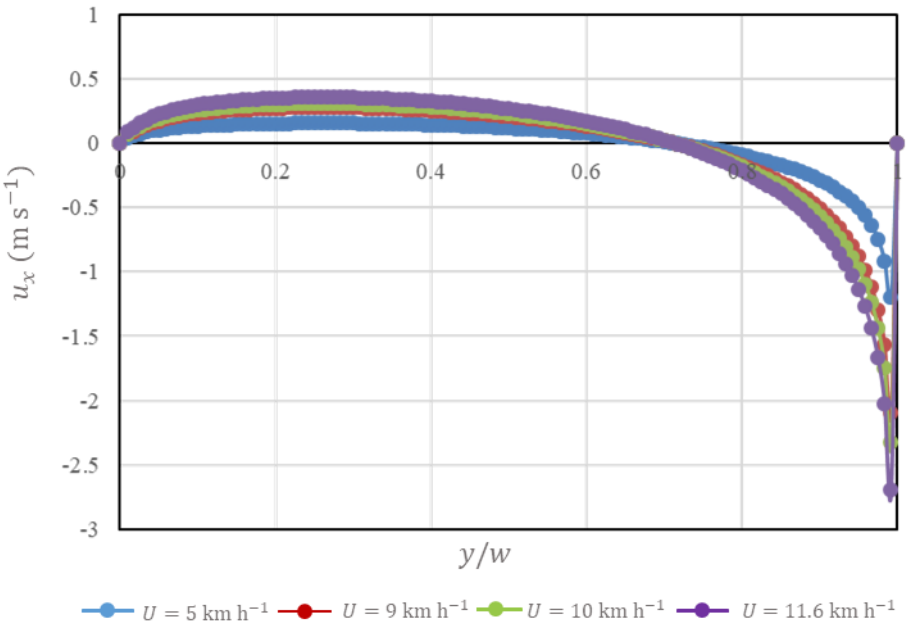


Figure 12. x-velocity at the window for single sided ventilation and $U = 5\ km\ h^{-1}$(blue); $U = 9\ km\ h^{-1}$(red); $U = 10\ km\ h^{-1}$ (green); $U = 11.6\ km\ h^{-1}$(purple)

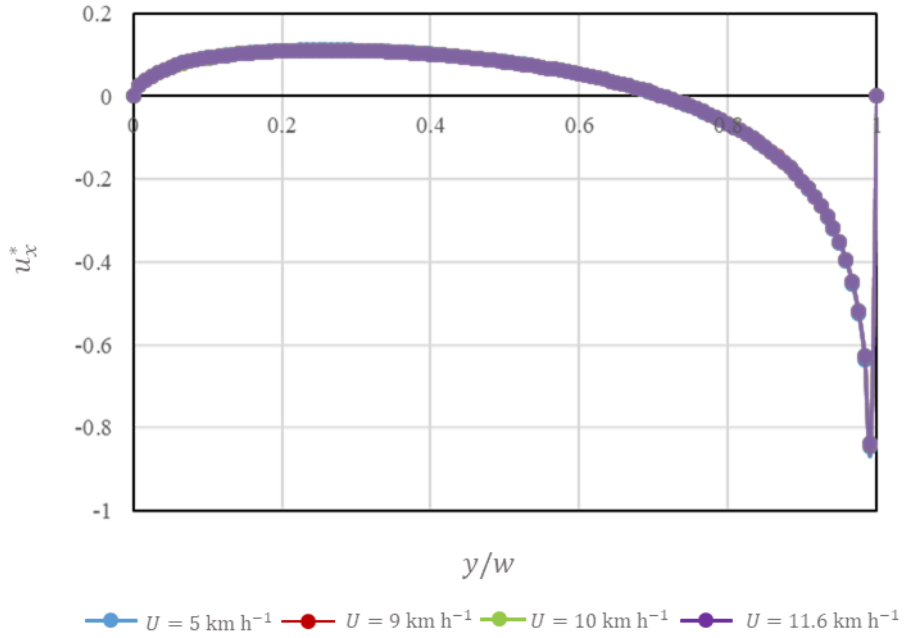


Figure 13. Normalized x-velocity at the window for single sided ventilation and different U.

As mentioned in Section 2.1, Warren (1977) reported a range of 0.022-0.026 that can be used to predict the exchange rate with a single windward opening of a building from Equation (3). Considering a room's depth of $1\,\mathrm{m}$ in 2D CFD simulations, as reported by ANSYS Fluent guidelines, the value Q^* was calculated for all of four cases. The value obtained was 0.058, which is roughly double the value reported by Warren (1977) . However, this was determined using a simplified 2D case, where the effect of the sides of the window is not considered.

3.2.2 Effect of Room Dimensions

In this section, the effect of the room's dimension, namely, the length and height, on the ventilation rate are studied. The simulations were step up with the same conditions as described in Section3.1.1. Three CFD simulations were performed changing the room's length $L = 4\,\mathrm{m}$, $L = 5\,\mathrm{m}$ and $L = 5.95\,\mathrm{m}$. The last value is the measured length of a classroom of a primary school in Porto, used as case study. Figure 14 shows the x-velocity at the window for these cases and the base case. It is clear that the profile and the ventilation rate are independent of the room's length.

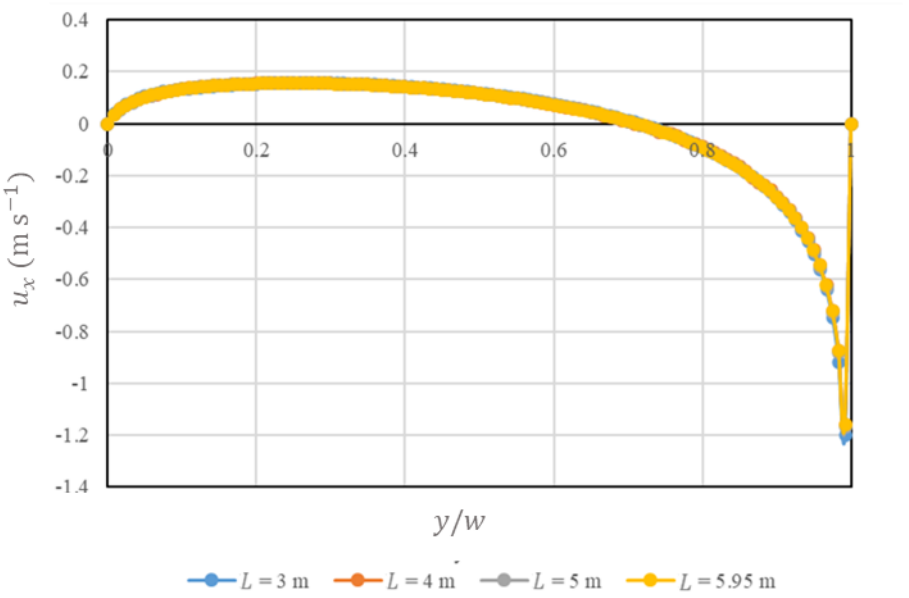


Figure 14. x-velocity at the window for single sided ventilation and $L = 3\ m$ (blue); $L = 4\ m$ (orange); $L = 5\ m$ (gray); $L = 5.95\ m$ (yellow)

The effect of the room height was also studied. In this case, since most classrooms have a standard height of 3.2 m, as define by (EPE 2017) , only two cases were considered, 3 m and 3.2 m. It is important to mention that changing H, the overall size of the domain also increases since there a relationship between the room's height and the atmosphere's height (3*H*), as described in Section 3.1.1. Figure 15 shows the velocity profile for both cases.

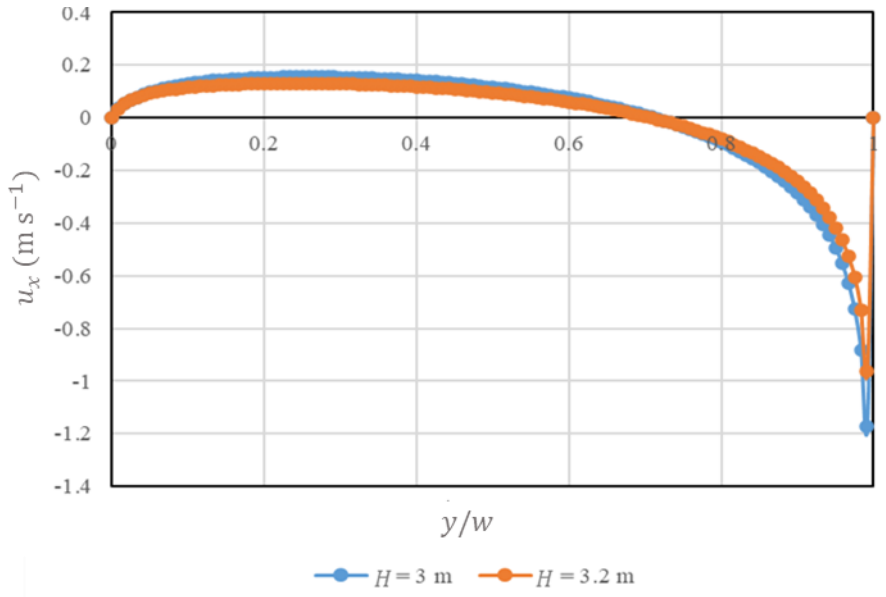


Figure 15. x-velocity at the window for single sided ventilation and $H = 3\ m$ (blue); $H = 3.2\ m$ (orange)

Although not too different the profile for the larger room is less steep than the profile for the base case ($H = 3\ \mathrm{m}$): for example, the maximum velocity value for the inlet part of the window is 15 % lower on the $H = 3.2\ \mathrm{m}$ case and the maximum negative velocity is 17 % lower. This indicates that the ventilation rate is influenced by the height of the room. However, it is not the volume of the room that is important, since increasing the length did not change the profile as seen above. In fact, it seems that the important factor is the distance to the walls, in this case to the top of the room. The influence of the distance to the solid walls is better described in the next section, when changing b.

3.2.3 Effect of Window Dimensions

The final two parameters studied were the window size and window position within the wall. The case described in section 3.1 has an opening of $0.6\ \mathrm{m}$, which is quite a small window for a typical classroom. To study the effect of the opening in the ventilation rate, two simulations were performed, increasing the size of the window to $1\ \mathrm{m}$ and $1.5\ \mathrm{m}$. Figure 16 shows the x-velocity at the window. The main difference between the three profiles is in the outflow near the top of the window. The larger windows show a higher velocity, the maximum velocity increases 24 % and 34 % when increasing w to $1\ \mathrm{m}$ and $1.5\ \mathrm{m}$, respectively, and so increasing the size of the opening also increases the ventilation rate, as expected. Once again, it seems that the air leaves the room only by the approximately top 30 %, although for the 2 larger windows this value decreases to 28 % and 25 %.

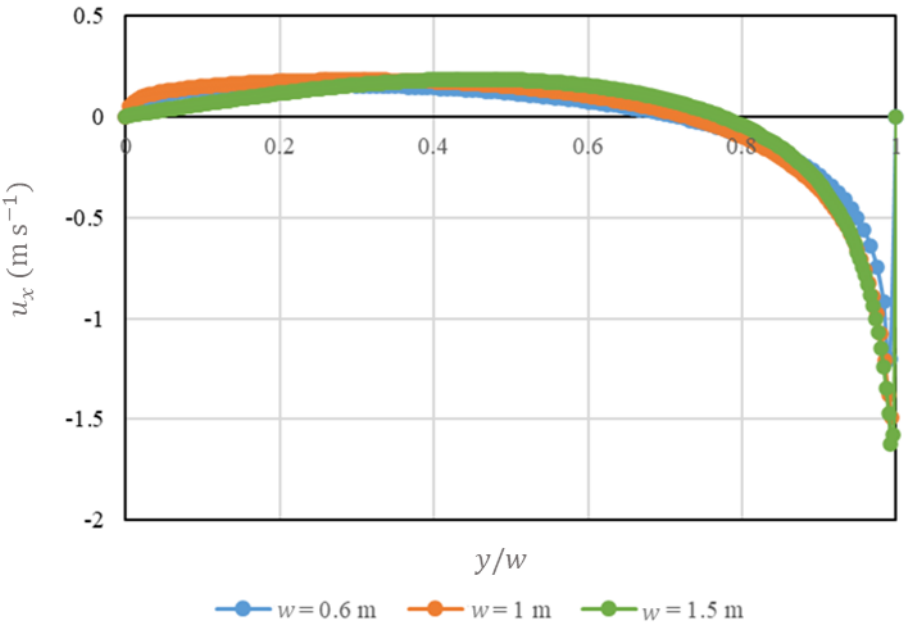


Figure 16. x-velocity at the window for single sided ventilation and $w = 0.6\ m$ (blue); $b = 1\ m$ (orange); $w = 1.5\ m$ (green)

The dimensionless outflow was calculated from Equation (3), and the values are shown in Table 3. The values show that Q^* is not constant with varying opening area.

Table 3. Dimensionless outflow for 2D simulations with varying window size

Simulation	Q^*
$w = 0.6$ m	0.058
$w = 1$ m	0.073
$w = 1.5$ m	0.069

Finally, the position of the window was also studied by changing the distance between the top of the window and the top of the building. Figure 17 shows the velocity profiles, where it is clear that the closer the window is to the top of the building, the larger the maximum velocity is, especially at the outflow jet: for example, for the $b = 0.2$ m and $b = 0.1$ m cases, there is an increase of 10 % and 24 %, respectively. Two factors probably contribute for this difference: first due to the acceleration near the top of the building as evidenced by the streamlines in Figure 3; second the effect that the top corner has, since it promotes a recirculation zone, also seen in Figure 3. It is also interesting to mention that between the cases with $b = 0.1$ m and $b = 0.01$ m there is very little difference, mean difference of 8 %, which suggests that for smaller values of b, the corner effect does not change much.

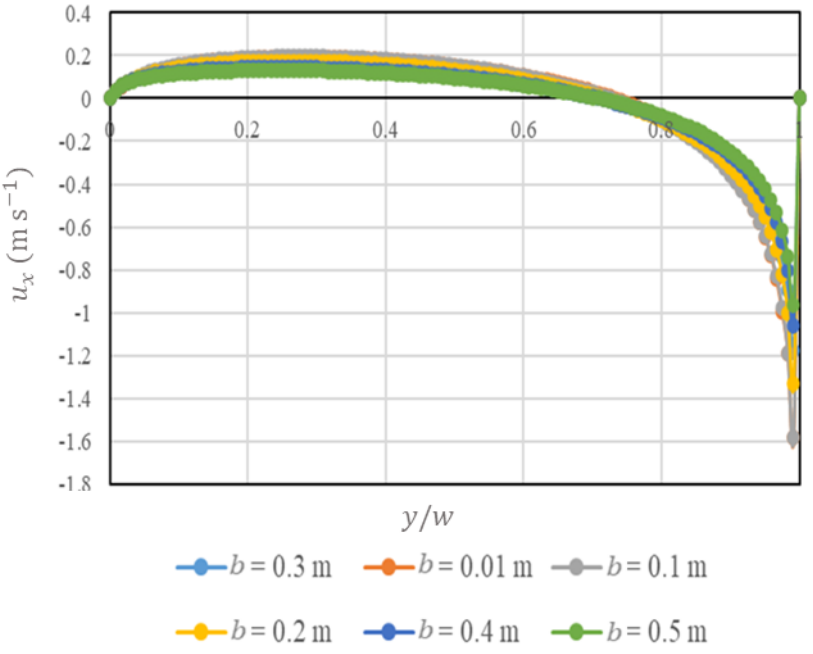


Figure 17. x-velocity at the window for single sided ventilation and: $b = 0.3\,m$ (blue); $b = 0.1\,m$ (red); $b = 0.01\,m$ (green); $b = 0.2\,m$ (purple); $b = 0.4\,m$ (cyan); $b = 0.5\,m$ (orange).

From this study, two main conclusions can be drawn. It became clear that the shape of the velocity profile at the window that is described by air entering through the lower part of the window and leaving in the form of a jet by the top 20-30 %, is independent of the parameters studied. Moreover, from the parameters under study, the wind velocity and window size are those that showed more impact on the ventilation rate.

3.3 CO_2 Tracer Simulations

The previous section discussed the effect of some design parameters on ventilation. However, the efficiency of ventilation in removing aged air from the room was not studied. Thus, tracer simulations were performed where the room was filled with a tracer gas, in this case CO_2, and then its concentration was monitored.

3.3.1 Setup and Solution Methodology

The RNG converged solutions of the previous section were used as initial condition in CFD simulations. The simulation was run at transient state and the species transport activated. The mass transfer was simulated using the convection-diffusion equation which is given by

$$\frac{\partial c}{\partial t} + \frac{\partial}{\partial x_j}(cu_i) = \frac{\partial}{\partial x_j}\left[\left(D + \frac{\mu_t}{\rho Sc_t}\right)\frac{\partial c}{\partial x_j}\right] \quad (19)$$

Where c is the concentration of a chemical species, in this case, CO_2 and D the mass diffusion coefficient. Sc_t is the turbulent Schmidt that takes the default values of 0.7.

CO_2 was introduced as a tracer fluid with $\rho_{CO2} = 1.98\ \mathrm{kg\,m^3}$and $\mu_{CO2} = 1.37 \times 10^{-5}\ \mathrm{Pa\,s}$. The diffusivity of CO_2 in the air was set as $D_{CO2/air} = 1.6 \times 10^5\ \mathrm{m^2 s^{-1}}$.

As mentioned in section 2, after a 2-hour long class with 25 students a classroom has approximately $8\ \mathrm{g\,m^{-3}}$, which corresponds to a mass fraction of CO_2, x_{CO2}, of 0.007. This value was determined using the human breathed out rate of CO_2, E_p $[\mathrm{L min^{-1} person^{-1}}]$, that depends on the person's weight, height, age, gender, and metabolic activity that can be estimated by

$$E_p = \frac{0.1656\ C_r\ A_s\ m_{eq}}{0.23C_r + 0.77} \quad (20)$$

where C_r is the respiratory coefficient, which takes the value of 0.83, A_s the skin area given by Dubois method ($A_s = 0.20247\ {h_p}^{0.725}\ {w_p}^{0.425}$, where h_p and w_p are respectively the person's height and weight) and m_{eq} the metabolic equivalent(Batterman 2017).

For the total simulation time, a 30 min break was considered. The final objective of this study was to report, using a 2D model, if a 30 minutes school break is enough to decrease the CO_2

concentration to the protection limit, which is $x_{CO2}^{Limit} = 0.002$. The time step size in this simulation was the same as the one used for the LES simulations in section 3.1.3.2.

3.3.2 Results and Discussion

Figure 18 shows the average mass fraction of CO_2 inside of the room for the base case, described in section 3.1, that is, a single room with $H = L = 3\ \mathrm{m}$, $U = 5\ \mathrm{km\ h^{-1}}$ and $w = 0.6\ \mathrm{m}$. The black line also shown in the figure corresponds to the protection limit. Results show that, in this case, the ventilation is enough to decrease the concentration to a value below the protection limit. However, at the end of 30 min, the CO_2 mass fraction is still 0.001.

The history of CO_2 in a room is fitted by an exponential curve to the data points, represented by a blue dotted line in Figure 18. The expression that gives the best trendline of for CFD data was determined from the method of least squares in Microsoft Excel and is given by

$$x_{CO2} = x_{CO2}^{0}\ \mathrm{e}^{-A_1 t} \qquad (21)$$

where A_1 is a constant.

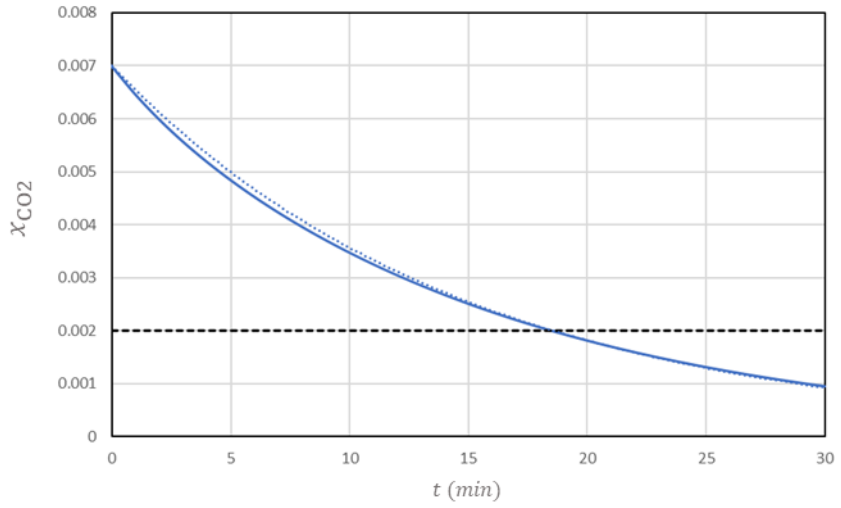


Figure 18. Average CO_2 mass fraction history for the base case. $U = 5\ km\ h^{-1}$ and $w = 0.6\ m$

Equation 21 is similar to the response of a Continuous Stirred Tank Reactors (CSTR) to a Heaviside step perturbation: $x_{CO2}^{0}(t) = x_{CO2}^{0}[1 - \mathrm{H}(t - 0)]$, in other words, it is equivalent to the Danckwerts $\mathrm{F}(t)$ curve for CSTR, given by

$$\mathrm{F}(t) = \frac{x_{CO2}}{x_{CO2}^{0}} = \mathrm{e}^{-\frac{t}{\tau_{vent}}} \qquad (22)$$

with

$$\tau_{vent} = \frac{V}{Q_{vent}} \qquad (23)$$

For these conditions, the residence time inside the room is $14.70\ \mathrm{min}$, and so the ventilation flowrate is $Q_{vent} = 9.90 \times 10^{-3}\ \mathrm{m^3 s^{-1}}$.

The efficiency of ventilation can be analysed from the flowrate that contributes to the removal of aged air. The flowrate percentage that contributes to the removal of aged air, $\%Q_{eff}$, is given by

$$\%Q_{eff} = \frac{Q_{vent}}{Q_{\mathrm{total}}} \times 100 \qquad (24)$$

where Q_{total} calculated integrating the velocity profile at the fraction of window's area that corresponds to the outlet. The integral of the total flow rate is calculated using the ANSYS Fluent numerical tools, which consider a standard depth of $1\ \mathrm{m}$.

The ventilation rate can also be estimated by determining the percentage of CO_2 that is removed at the end of the $30\ \mathrm{min}$, $\%vent$, which is given by

$$\%vent = \frac{x^0_{\mathrm{CO2}} - x^{t=30\ \mathrm{min}}_{\mathrm{CO2}}}{x^0_{\mathrm{CO2}}} \times 100 \qquad (25)$$

Table 4 shows the $\%Q_{eff}$ and $\%vent$ for the base case conditions.

Table 4. 2D Simulation Results and Ventilation metrics

Condition	τ_{total} (min)	Q_{total} ($\mathrm{m^3 s^{-1}}$)	τ_{vent} (min)	Q_{vent} ($\mathrm{m^3 s^{-1}}$)	$\%Q_{eff}$	$\%vent$
Base Case: $U = 5\ \mathrm{km\ h^{-1}}$ $w = 0.6\ \mathrm{m}$	3.08	4.9×10^{-2}	14.70	9.90×10^{-3}	20.9	86.5
$U = 9\ \mathrm{km\ h^{-1}}$	1.72	8.7×10^{-2}	8.85	1.70×10^{-2}	19.5	96.6
$U = 11.6\ \mathrm{km\ h^{-1}}$	1.33	0.11	6.70	2.18×10^{-2}	19.4	98.7
$w = 1.5\ \mathrm{m}$	1.05	0.14	5.81	2.58×10^{-2}	18.0	99.4

This analysis was also made for the three more cases in section 3.2, $U = 9\ \mathrm{km\ h^{-1}}$, $U = 11.6\ \mathrm{km\ h^{-1}}$ and $w = 1.5\ \mathrm{m}$. Figure 19, Figure 20 and Figure 21 show the average CO_2 concentration history for these conditions in the form of the Danckwerts $\mathrm{F}(T)$ curve, the protection limit (normalized by the initial mass fraction) is also represented in these Figures. Table 4 shows the values obtained for the four conditions. From the results it can be seen that when the flowrate, Q_{total}, increases so does the ventilation flowrate. However, it doesn't present a linear relation. The fourth simulation, $w = 1.5\ \mathrm{m}$, is the one that has a higher value of $\%vent$ which is consistent with the previous results. Comparing the velocity profiles of the simulations shown before in Figure 12 and Figure 16, the simulations with higher wind speeds

present higher velocity values, but this does not consider the ventilation area. The case with a larger opening has the highest ventilation rate showing the importance of the area in the effective ventilation of the room.

The $\%Q_{eff}$ for all cases is between 18-24 % which indicates that only one fourth to one fifth of the measure air flowrate actually contributes to the renewal of the indoor air. It is also interesting to note that for the cases where only the wind speed changes, the value seems to circle around 20-21 %.

For the three conditions, the ventilation was enough to reduce CO_2 concentration below the protection limit. But as seen above, the simulation with the larger opening has the most efficient ventilation.

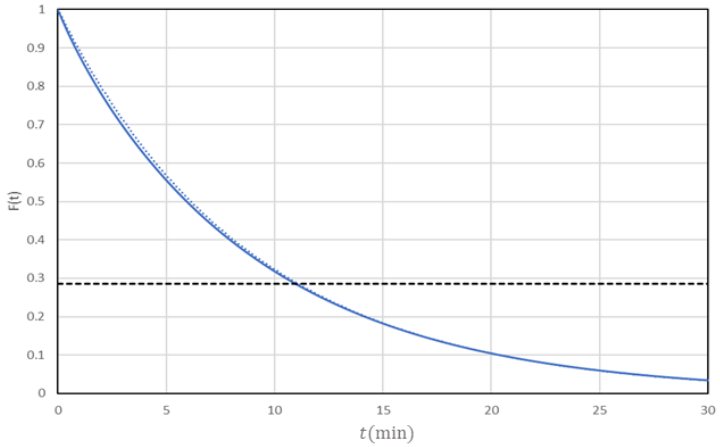


Figure 19. Danckwerts $F(t)$ curve for $U = 9\ km\ h^{-1}$, $w = 0.6\ m$. From a 2D simulation

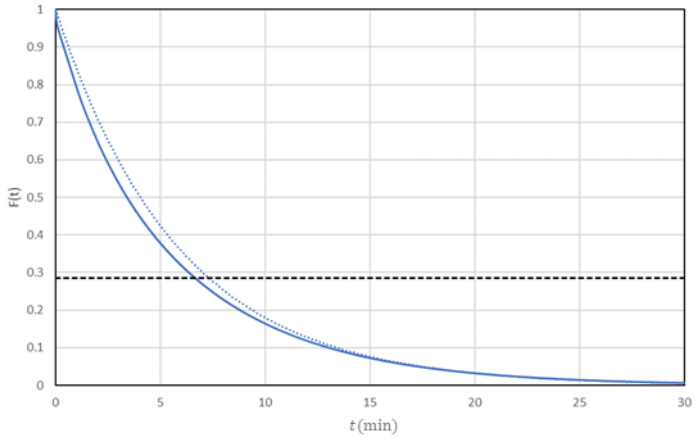


Figure 20. Danckwerts $F(t)$ curve for $U = 5\ km\ h^{-1}$, $w = 1.5\ m$. From a 2D simulation

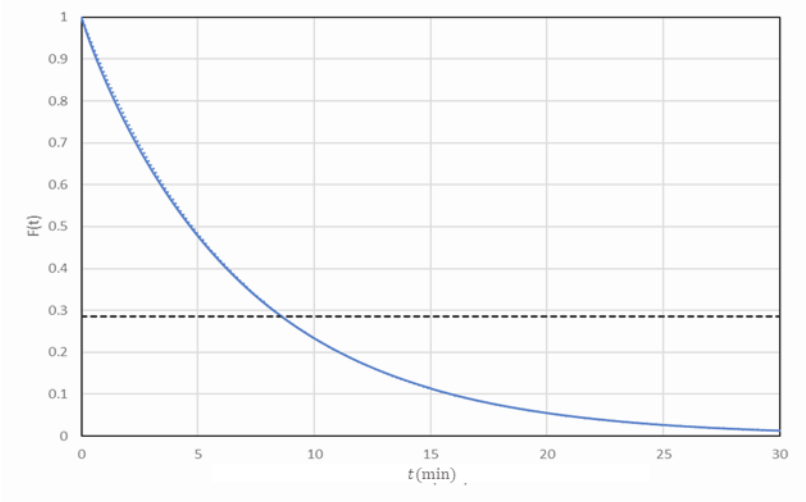


Figure 21. Danckwerts $F(t)$ curve for $U = 11.6\ km\ h^{-1}$, $w = 0.6\ m$. From a 2D simulation

Figure 22 shows the mass fraction contour map for the 1st case after 30 minutes. As expected by analysing the streamlines in Figure 3, the air near the wall is first renewed, and the centre of the room tends to stay at a higher concentration. This is mainly due to the principal mechanism responsible for renewing the air of the room, which is the turbulent dispersion between the air inside the room and the air outside the room. The dispersion transport of CO_2 occurs through the closed loops streamlines, and so the ones closer to the window have smaller concentrations of CO_2.

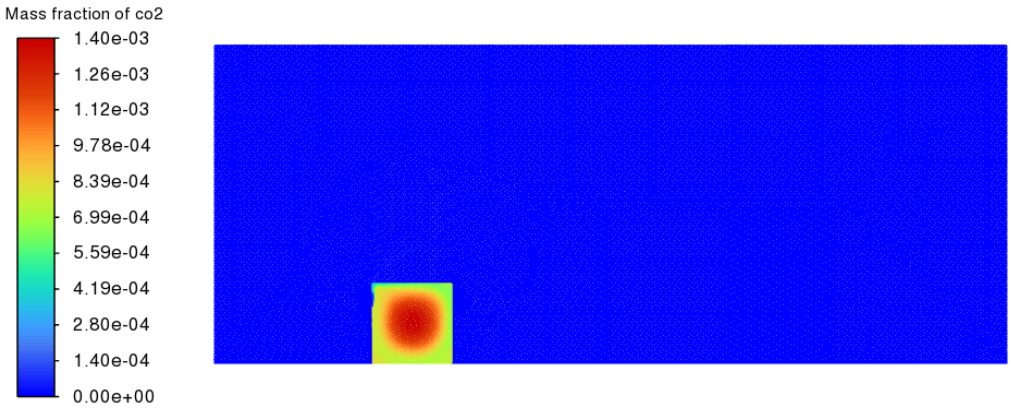


Figure 22. Mass fraction of CO_2, x_{CO2}, contour map for the base case at $t = 30\ min$.

According to Equation (22), the ventilation rate should not be dependent on the initial CO_2 concentration. This was verified from the simulation of other initial concentrations of CO_2, namely 0.003 and 0.025. From the fitting of data points, τ_{vent}, $\%Q_{eff}$ and $\%vent$ were determined and reported in Appendix A

4 3D Simulation of Natural Ventilation

The natural ventilation in classrooms is also studied in this work using a 3D CFD simulations. This section is divided into two parts: the first is the simulation of half of the room domain (symmetric domain) to save computational resources and the second part addresses the flow in an entire room. 3D CFD flow was simulated using ANSYS Fluent 2021.

4.1 3D Symmetric CFD model

The CFD simulation with half of the domain considers the 2D geometry of Figure 1 as the symmetry plane of the room. The dimensions were chosen to create a room with the same proportions as a typical classroom. Figure 23 and Figure 24 show the geometry and the respective dimensions. For this case, $L = H = 3\,\mathrm{m}$, $L_{3D} = 10\,\mathrm{m}$, $H_{3D} = 12\,\mathrm{m}$, $s = 0.72\,\mathrm{m}$, $w = 0.6\,\mathrm{m}$ and $l = 0.32\,\mathrm{m}$. The mesh was created using a hex dominant method with an element of size $0.067\,\mathrm{m}$ and $0.005\,\mathrm{m}$ at the window. For the region surrounding the room, a multizone method was used.

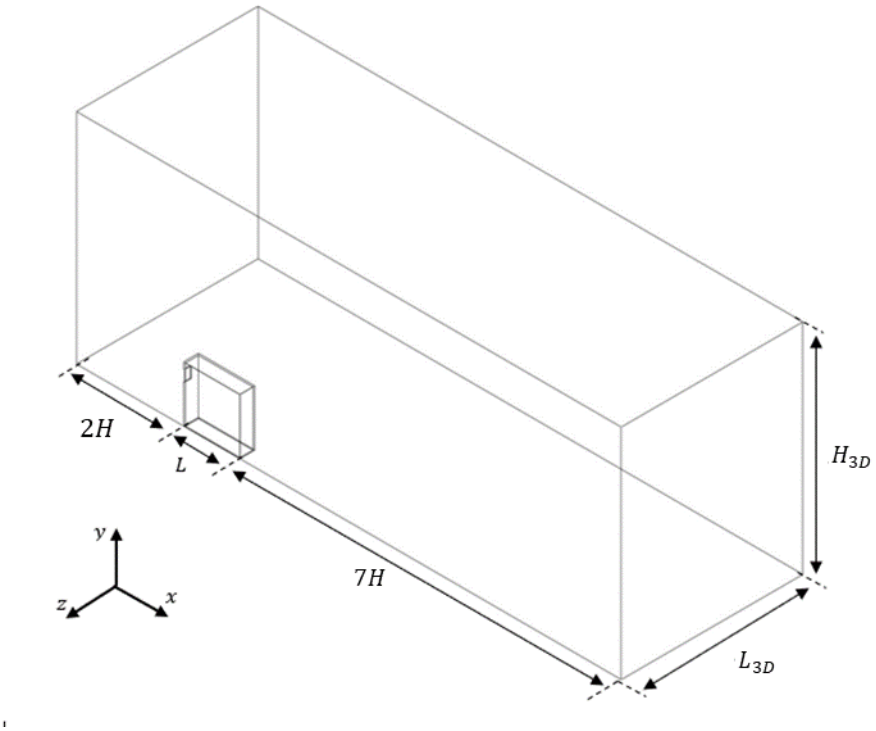


Figure 23. 3D CFD geometry considering half of the physical domain.

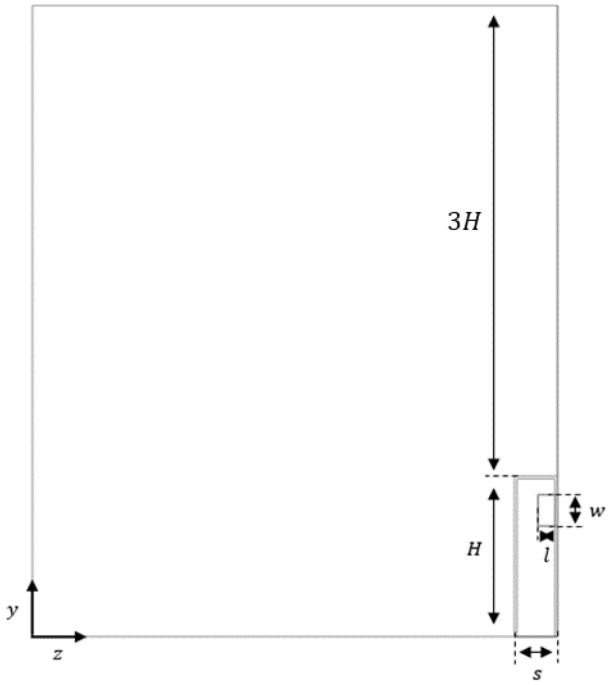


Figure 24. Front view of 3D half geometry.

Regarding the case setup, the steady-state simulation was set using the following models and boundary conditions: standard k-ε model, inlet with a constant wind front equal to $5\ \mathrm{km\ h^{-1}}$, $Ks = 6 \times 10^{-4}\ \mathrm{m}$, 4 % of TI, pressure outlet condition at the right wall, symmetry on the top and lateral boundaries and wall on the bottom and on the surfaces of the room. For all 3D simulation the convergence criteria considered was the stabilization of the residuals.

A mesh independence test was performed by refining the cells with a y^+ at the buffer layer, that is, 5 to 30. The first, with 4 levels of refinement, had only 7 % more cells, and so it was considered to be insufficient. The other refinement was performed employing 6 levels, resulting a mesh with 37 % more cells than the original. Analysing the velocity profile at the window, Figure 25 shows that this refinement did not significantly increase the number of elements at the window, and so, the top of the window, which corresponds to the outlet of the indoor air, could still be under simulated. For this reason, the mesh was further refined at the window. First, a mesh with 2 230 032 cells was obtained with 6 levels of refinement, Mesh 3DS_2M, where the S stands for symmetric, and another mesh was generated with 3 319 435 cells, Mesh 3DS_3M. These last two meshes produced very similar results; the maximum difference was less than 7 %, so Mesh 3DS_2M was considered.

Figure 25 shows the x-velocity profiles at the window for Mesh 3DS_2M at $z = 10\ \mathrm{m}$ (symmetry plane) as well as the profile of the 2D simulation described in section 3.1.3. The velocity profile of the 3D simulation shows that the air enters the room by the lower part of the window and leaves through a fraction of window area of 22.5 %. The ratio of between the air inlet and outlet for the 2D and the 3D is similar but in the 3D case it is roughly 8 % smaller. Figure 25 also shows that the velocity magnitude of the outlet jet velocity in 3D simulation is much smaller (≈80 %) than in 2D simulation, due to the effect of the side walls that is not considered in a 2D simulation. In the region next to the wall, the velocity profile determined from 3D simulations is quite abrupt compared to the 2D simulation.

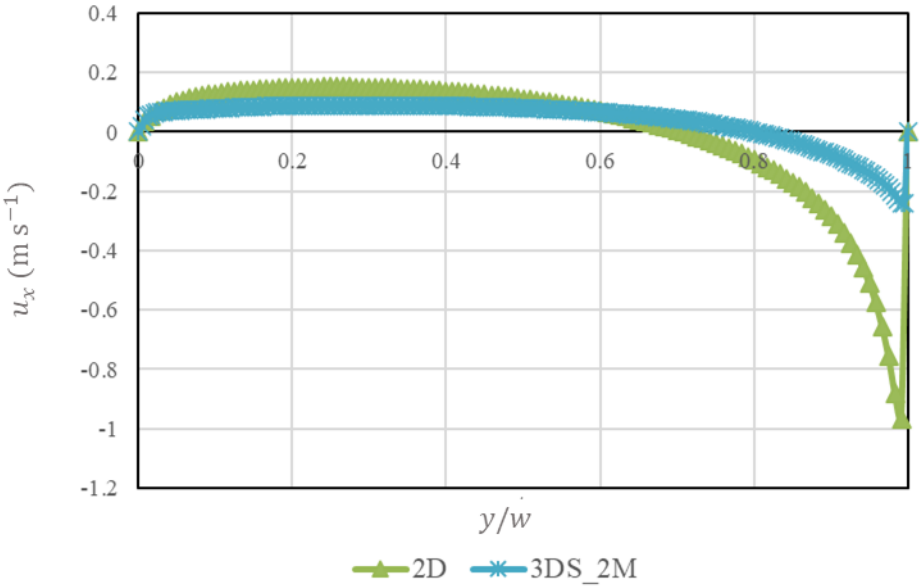


Figure 25. x-velocity profile at $z = 10\ m$: 2D (green); Mesh 3DS_2M (blue) for 3D symmetric domain simulation. case ($U = 5\ km\ h^{-1}$, $w = 0.6\ m$).

The x-velocity profile at the center of the window ($y = 2.4\ \mathrm{m}$) is shown in Figure 26. This figure shows the velocity profile of the half window since $z/l = 0$ corresponds to symmetry boundary condition. This figure also shows that most of the window length, (83 % of the total window area) corresponds to an inlet, and, near the wall, there is an outflowing stream of air. However, the zone near the wall is also quite abrupt.

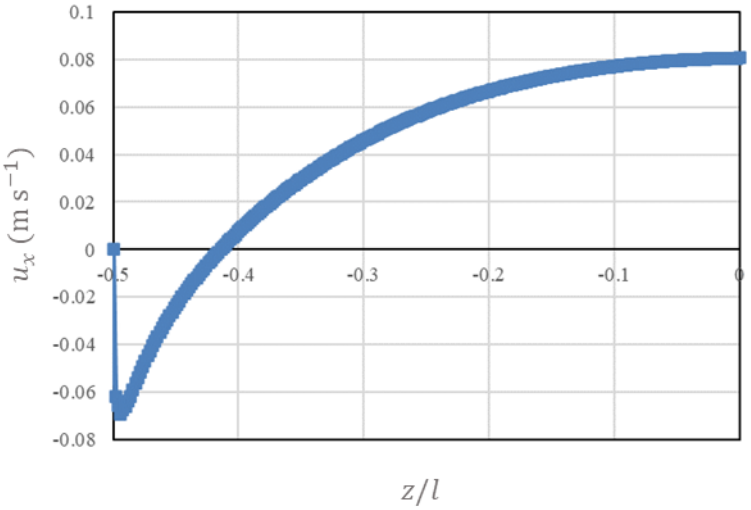


Figure 26. x-velocity profile at $y = 2.4\ m$ for a 3D symmetric domain simulation. case ($U = 5\ km\ h^{-1}$, $w = 0.6\ m$).

4.1.1 Comparison with RNG model

According to the literature, the solution of 3D flow using standard k-ε model is not the most suitable. Since RNG model is the preferred model, a steady state simulation was performed. Nevertheless, RNG solution did not converge for the criteria mentioned before. An extra refinement was done, considering the cells with high mass imbalance creating a mesh with 3 375 533 cells, but it still did not converge, since the residuals did not stabilize.

The convergence issues should occur due to the lack of symmetry of the flow. And so, another CFD model considering the entire domain was developed in Section 4.2.

4.2 3D CFD Simulation - Full domain

Figure 27 and Figure 28 show the geometry and the respective dimensions. For this case, $L = H = 3\ \mathrm{m}$, $BH = 9\ \mathrm{m}$, $L_{3D} = 20\ \mathrm{m}$, $H_{3D} = 12\ \mathrm{m}$, $s = 1.44\ \mathrm{m}$, $w = 0.6\ \mathrm{m}$ and $l = 0.64\ \mathrm{m}$. The setup for these simulations, including the boundary conditions and the models, was identical to the model described in section 4.1.

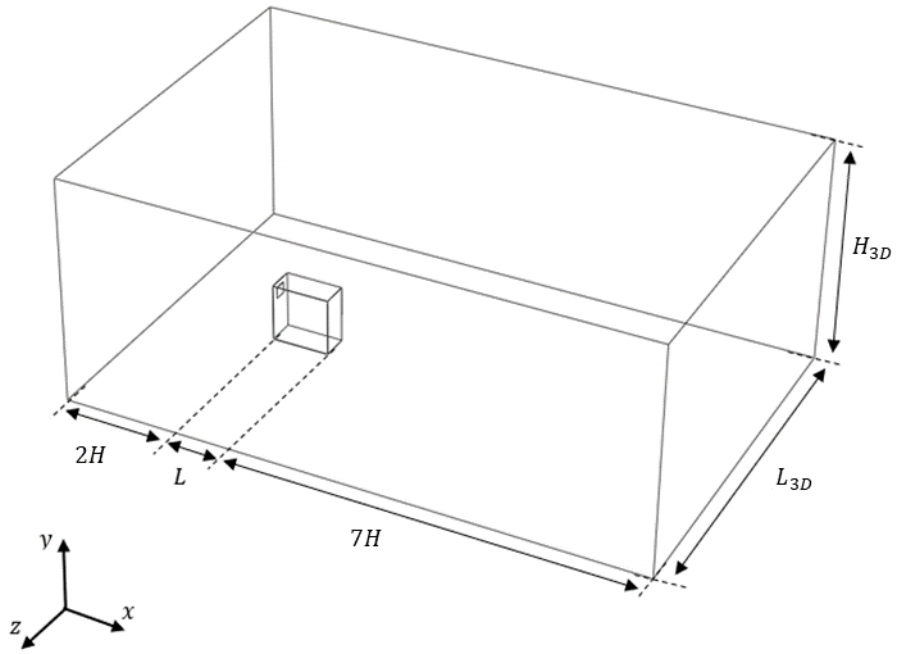


Figure 27. 3D Geometry for the full domain.

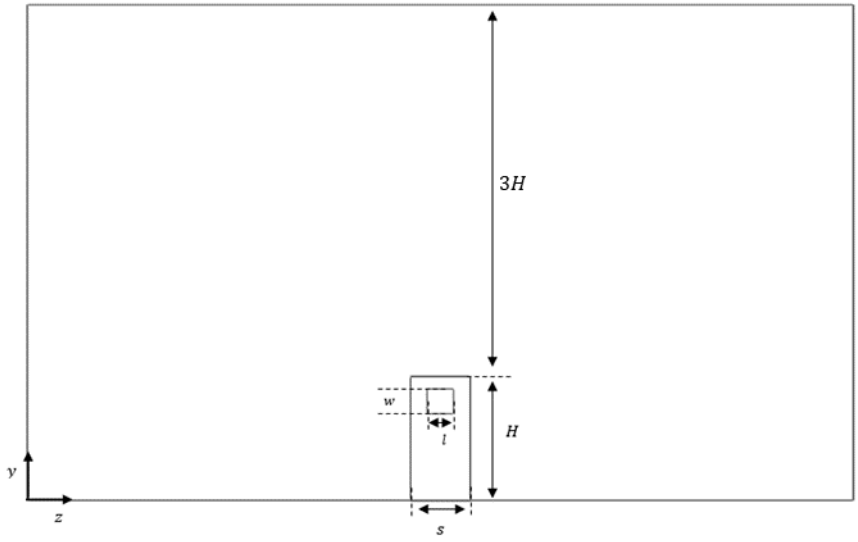


Figure 28. 3D Geometry for the full domain. Front view.

4.2.1 Mesh Independence test

The mesh was generated using a smaller element size for the room and increasing its size in the surroundings. A mesh independence test was done using four meshes with an increasing number of elements, 3DF_iM, with F standing for Full and i for the number of mesh elements, rounded to the millions. The mesh independence study consisted of the simulation of flow at

single sided ventilation, using the standard k-ε, and the comparison of the average x-velocity at the windward opening, $\bar{u}_x$, for the four meshes. Table 2 shows the CFD results of the average x-velocity. Meshes 3DF_3M and 3DF_6M show less than a 1.5 % variation while 3DF_6M and 3DF_15M less than 0.2 %. However, this increase in accuracy was considered not relevant regarding the increase of computational resources needed to simulate 3DF_6M. Therefore, 3DF_3M was considered the valid CFD model.

Table 5. Mesh Independence test for the full 3D domain

Mesh	Elements	$\bar{u}_x$
3DF_2M	2 228 695	3.74×10^{-2}
3DF_3M	3 303 540	4.72×10^{-2}
3DF_6M	6 579 225	4.65×10^{-2}
3DF_15M	15 974 610	4.64×10^{-2}

4.2.2 Results and discussion

Figure 29 shows the x-velocity profile at $z = 10\,\mathrm{m}$ for 3DF_3M. Figure 29 also shows the x-velocity profile at $z = 10\,\mathrm{m}$ determined from simulation using half of the domain. The comparison between both profiles shows that the maximum velocity magnitude in both CFD models is in the same range. However, in CFD model using the full domain, the velocity profile is smoother near the wall. The same conclusion can be drawn by comparing the horizontal profile. Figure 30 shows the x-velocity profile for a horizontal line (z-direction) at the center of the window ($y = 2.4\,\mathrm{m}$).

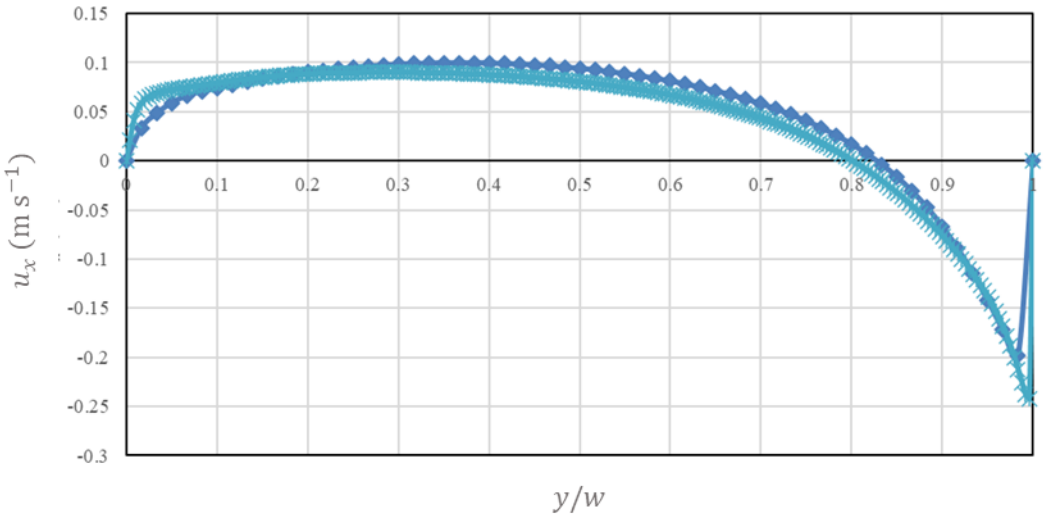


Figure 29. x-velocity profile of $z = 10\ m$, from 3D simulations: 3DF_3M (blue); 3DS_2M (cyan).

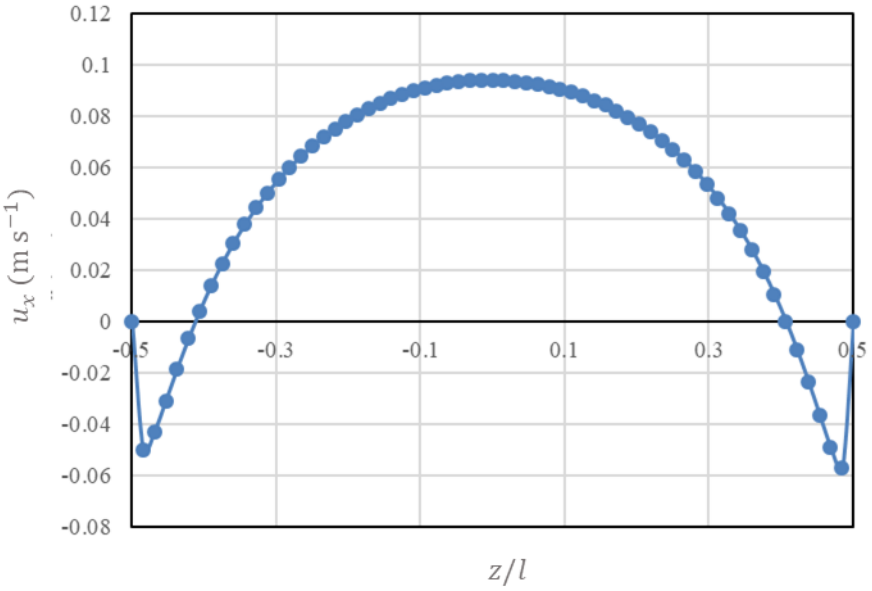


Figure 30. x-velocity profile at $y = 2.4\ m$. from 3D simulation of full domain

4.2.2.1 Comparison with RNG model

Results obtained from standard k-ε model were compared to the results using RNG model. The convergence criteria were set as the residuals' stabilization. Contrary to the results using half of the domain, the simulation using the full domain converged for the convergence criteria.

The flow structure of the air outside the room can be visualized by plotting pathlines in the Fluent software, this plots are presented in Appendix B . Figure 31 and Figure 32 show the x-velocity profile at $z = 10\ \mathrm{m}$ and at $y = 2.4\ \mathrm{m}$. The comparison of both models shows that RNG

model produced a smoother profile that seems to better capture the jet velocity. As mentioned before, the RNG models is preferred in the literature and so further simulations use this model (Zhang, Weerasuriya, and Tse 2020).

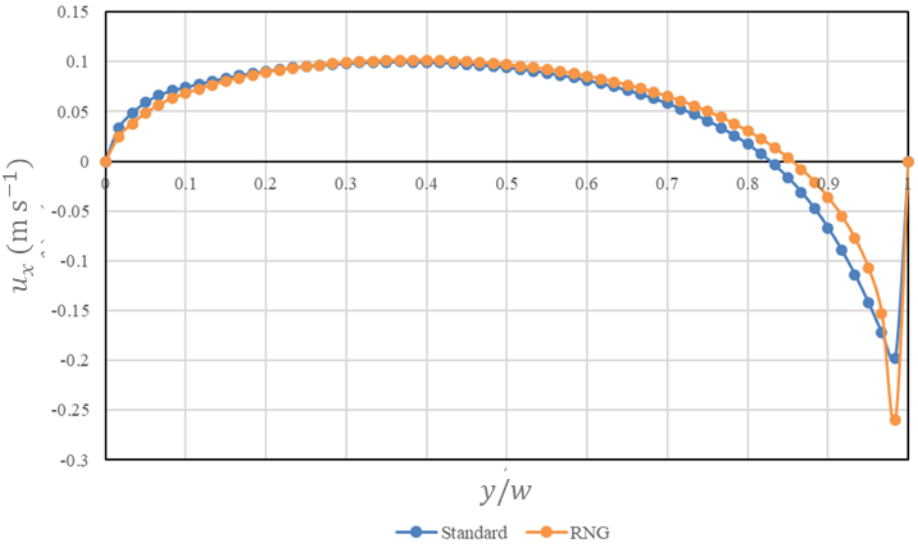


Figure 31. x-velocity profile of the window at $z = 10\ m$: Standard k-ε model (blue); RNG model (orange).

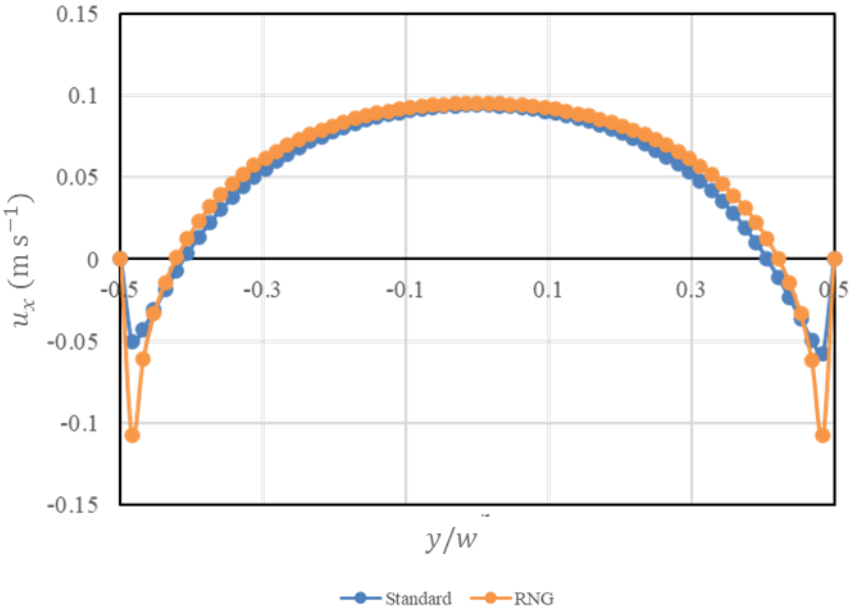


Figure 32. x-velocity profile at at $y = 2.4\ m$: Standard k-ε model (blue); RNG model (orange).

The analysis from the velocity profiles shows that the air enters the room by the bottom and middle of the window while it leaves as a jet at the top, left and right window's wall. Figure 33 shows the x-velocity contour map at the window and the same analysis made from Figures

31 and 32 can be concluded. Moreover, the velocity at the corners at the top of the window has a higher magnitude.

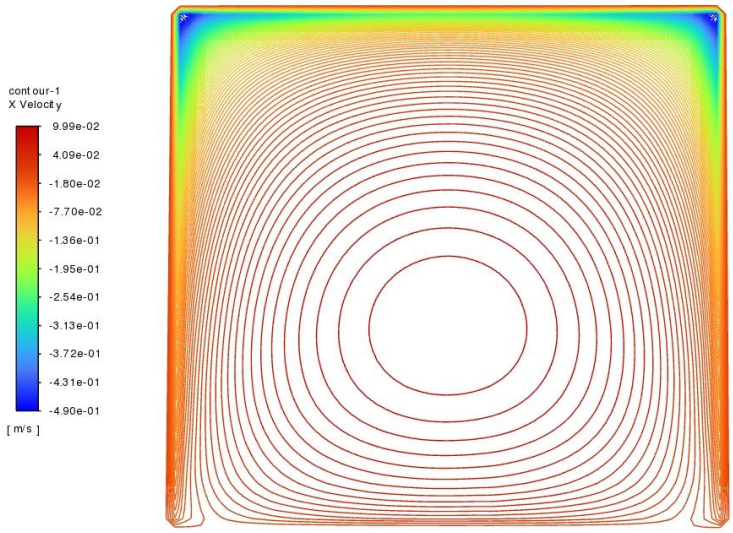


Figure 33. x-velocity contour at the window from a 3D simulation.

4.2.2.2 Ventilation Parameter Study

Three different conditions were studied to compare to the 2D CFD simulation: $U = 9\ \mathrm{km\ h^{-1}}$, $U = 11.6\ \mathrm{km\ h^{-1}}$ and $w = 1.5\ \mathrm{m}$. Q^* was calculated using Equation (3), and the results are in Table 6. Similar to the 2D results, the flowrate seems to be linearly correlated with the wind speed but not with the opening area, since the values for the dimensionless out flowrate are constant while increasing U, but now when increasing A. In spite of showing the same behaviour, the 2D and 3D CFD models do not show a straightforward correlation. This indicates that, the 2D cases cannot be used as a cost-effective alternative to quantify and study indoor ventilation. However, they can still be useful to discern some behaviour, namely the effect of some parameters, e.g., wind speed, window height and position, etc.

Table 6. Dimensionless out flowrate for 3D cases

Simulation	Q^*
Base Case: $U = 5\ \mathrm{km\ h^{-1}}$ $w = 0.6\ \mathrm{m}$	0.0263
$U = 9\ \mathrm{km\ h^{-1}}$	0.0253
$U = 11.6\ \mathrm{km\ h^{-1}}$	0.0263
$w = 1.5\ \mathrm{m}$	0.0477

The entire 3D CFD domain enables to access the effect of the room length on the flow structure through the window. Another domain with a room length of $s = 2\ \mathrm{m}$ was simulated. Figure 34 shows the x-velocity contour map at the window for this new case. Compared with Figure 33, it is clear the shape of the velocity profile is quite different. In base case ($s = 1.44\ \mathrm{m}$), the air leaves the room through the top and sides of the window while it enters via the center, while, in the new case ($s = 2\ \mathrm{m}$), the air leaves only from the top and the top half of the sides. This difference is probably due to the distance from room's walls to the window.

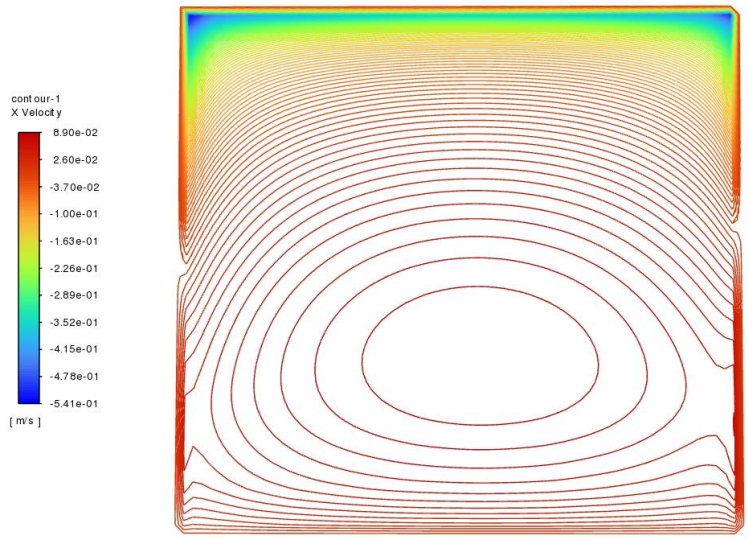


Figure 34. x-velocity contour map at the window for $s = 2\ m$ for a 3D simulation

However, it is only the shape that changes since the area of the window where the x-velocity is negative, that is where there is out-flow, is, in both cases, 0.1086 m^2, which corresponds to approximately 28 % of the total window area.

Performing the same analysis to the bigger window case ($1.5 \times 1.6\ \mathrm{m}$), the area ratio mentioned is approximate 33 %. These values are similar to the 30 % obtained from the 2D simulation mentioned in section 3.1.3. This indicates that the area percentage that serves as an outlet might be constant.

4.3 CO_2 Tracer Simulations

The ventilation efficiency of the 3D CFD model was studied using tracer simulations, setting CO_2 as the tracer gas. The simulations setup is identical to the description in section 3.3.1. Four simulations were performed, the base case ($U = 5\ \mathrm{km\ h^{-1}}$, $w = 0.6\ \mathrm{m}$), for a wind speed of 9 $\mathrm{km\ h^{-1}}$, wind speed of 11.6 $\mathrm{km\ h^{-1}}$ and larger window with $w = 1.5\ \mathrm{m}$. These simulations were run for the same conditions and geometric parameters as 2D CFD simulations.

The same model used in Section 3.3.2 was fitted to the results. Figure 35 shows the Danckwerts $\mathrm{F}(T)$ curve for the base case. Contrary to the 2D equivalent case, a school break of 30 min was not enough to decrease the concentration of CO_2 to below the protection limit but only to approximately 0.003. This was expected, since, as mentioned in Section 4.2.2, air-flow is lower in the 3D CFD model than in 2D simulations due to the effect of the side of the window and walls of the room.

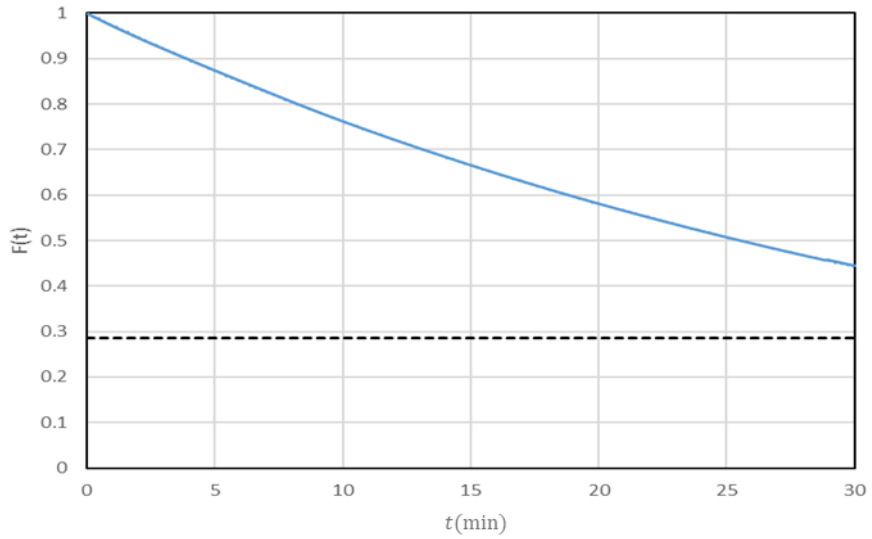


Figure 35. Danckwerts $F(t)$ curve for the base case ($U = 5\ km\ h^{-1}$, $w = 0.6\ m$). From a 3D simulation.

Nevertheless, as observed in 2D CFD simulations, the concentration history is described by the CTSR model. Moreover, the adjusted function, perfectly describes the simulated data, unlike the 2D simulation, where there was some deviation. The same metrics used for 2D CFD simulations, calculated with Equations (24) and (25) were used to quantify the ventilation efficiency. Table 7 shows the results obtained for all 3D simulations preformed.

Table 7. 3D Simulation Results and Ventilation metrics for 3D simulation of the entire 3D domain.

Simulation	τ_{total} (min)	Q_{total} ($\mathrm{m^3 s^{-1}}$)	τ_{vent} (min)	Q_{vent} ($\mathrm{m^3 s^{-1}}$)	$\%Q_{eff}$	$\%vent$
Base Case	15.42	1.4×10^{-2}	37.04	5.83×10^{-3}	41.6	55.5
$U = 9\ \mathrm{km\ h^{-1}}$	8.89	2.4×10^{-2}	20.00	1.08×10^{-2}	44.4	77.7
$U = 11.6\ \mathrm{km\ h^{-1}}$	6.63	3.3×10^{-2}	17.88	1.21×10^{-2}	37.1	81.4
$w = 1.5\ \mathrm{m}$	2.16	0.16	6.15	5.60×10^{-2}	35.2	99.2

Figure 36, Figure 37 and Figure 38 show the concentration history for the other cases reported in Table 7. For case $U = 9\ \mathrm{km\ h^{-1}}$ and $U = 11.6\ \mathrm{km\ h^{-1}}$, a 30 min break enables to decrease the concentration just below the protection limit while with the bigger window, the ventilation was almost complete, as shown in Figure 36.

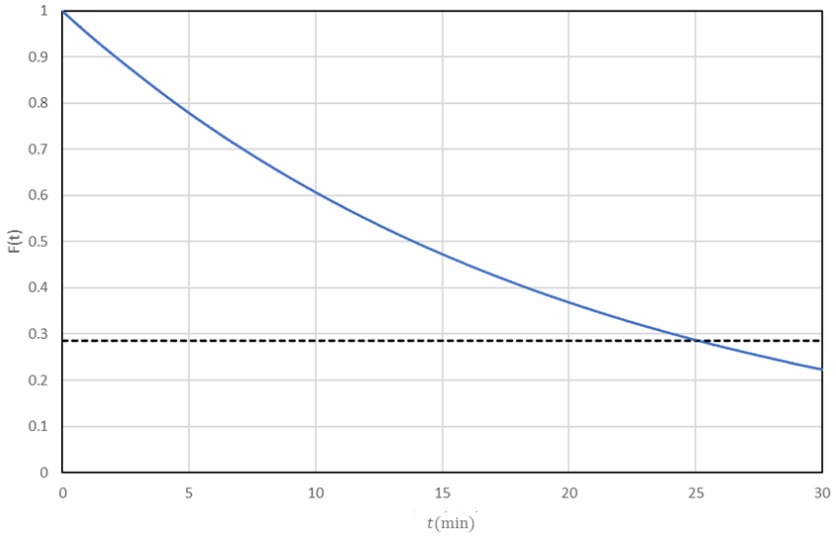


Figure 36. Danckwerts $F(t)$ curve for $U = 9\ km\ h^{-1}$ from a 3D CFD simulation.

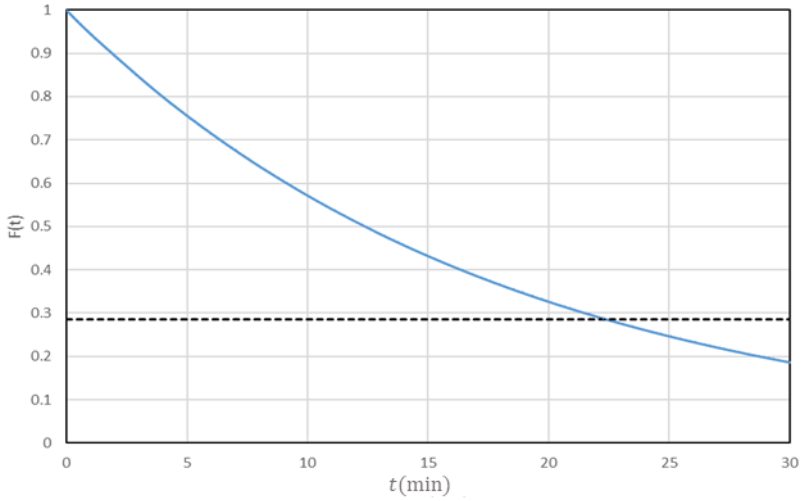


Figure 37. Danckwerts $F(t)$ curve for $U = 11.6\ km\ h^{-1}$ from a 3D CFD simulation.

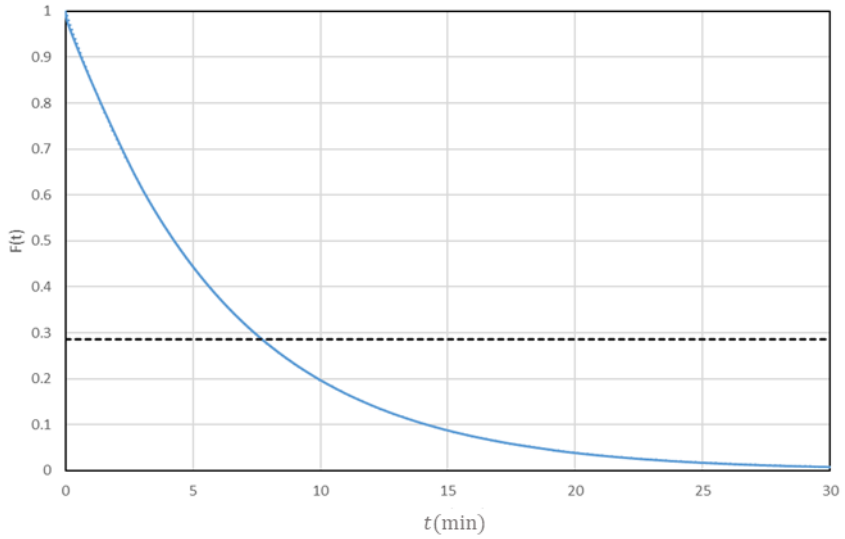


Figure 38. Danckwerts $F(t)$ curve for $w = 1.5\ m$ from a 3D CFD simulation.

Comparing these cases with the 2D CFD models, two important conclusions can be drawn. The 2D CFD simulation is not an adequate simplification of the 3D CFD model in terms of quantitative analysis of natural ventilation since there is no clear relation between both cases; However, it can still be useful to discern some behaviours since the qualitative interpretation of the results is quite similar. For example, for both the 2D and 3D CFD models, higher wind speeds lead to better ventilation but this increase is lower than the one obtained when increasing the window area. On the other hand, $\%Q_{eff}$ for 3D simulations seems to be approximately twice the value obtained from the 2D simulation, the mean value of the ratio of $\%Q_{eff}$ for the 2D simulations and for the four 3D simulations is 49.3 %. This clearly indicates that the relation between the out-flowrate and the effective ventilation is the same for both simulations.

5 Conclusions

The work presented in this thesis studied natural ventilation using Computation Fluid Dynamics (CFD). There are two main types of natural ventilation: wind-driven ventilation and buoyancy-driven ventilation. This dissertation focused on the study of the first one. The studies made throughout the work are preliminary studies for a case study of a real primary classroom from a school located in Porto.

In a first approach, several studies were made using a 2D CFD domain. First the effect of some of the simulation setup conditions on the converged solution was analysed. It was found that the wall roughness represented by Ks and the inlet turbulence conditions, i.e., TI did not affect the solution. The effect of the turbulence models was also studied, comparing standard k-ε, realisable k-ε, RNG and LES. For the 2D simulations the results obtained were equivalent.

To study the shape of the flow through the window, the x-velocity was plotted. It was found that most of the window (70 %-75 %) served as an inlet, where the air enters the room while from the top part of the window, the other 25 %-30 %, the air leaves the room in a shape of a jet.

To better understand the effect of some design parameters, namely the architecture of the room and window and the wind speed, on the ventilation, several 2D CFD simulations were performed. The results showed that the profile described above is always present, changing only the velocity magnitude. By calculating the dimensionless flowrate, it was found that the out-flowrate is linearly correlated with the wind speed. However, the same relation is not observed when changing the opening area. It was also found that the distance of the window to the room's walls significantly affected on the ventilation. Of all the design parameters studied the ones that have a larger impact were the wind speed and the window size.

In order to study the ventilation efficiency of the 2D cases, tracer simulations were performed. CO_2 was used as the tracer gas since it is one of the most important pollutants in the classroom context. It was found that only a small fraction of the flowrate (15 % to 25 %) contributed to the effective renewal of the indoor air. It was also found that the ventilation, that is the removal of aged air from the room can be well modelled by the Danckwerts $F(t)$ curve for CSTR. The results also showed that the air is renewed mainly by turbulent dispersion rather than convection.

After the first 2D approach, a 3D domain was studied. First, a 3D symmetric CFD domain was tested, but this presented convergence problems, so a full 3D CFD domain was studied. For the

3D case, it was shown that the RNG model produced different results from the standard, especially in the velocity profile near the window walls.

The results showed that the flow shape through the opening described with the 2D domain was still valid, but with smaller values of velocity. It was also found that for the overall window, the air left the room via 30 % of the window, manly at the top corners. The shape of the velocity contours at the opening was show to be related to the distance to the room's walls. However, the volume of the room did not influence the percentage of the window from where the air leaves.

Like what was done with the 2D domain, tracer simulations were performed to study the ventilation efficiency. From these results it was found that the percentage of the flowrate that effectively contributed for the renewal of the indoor air was higher than the reported by the 2D simulation. It was also found that $\%Q_{eff}$ for 3D cases seems to be double the value obtained from the 2D cases, the mean value obtained from comparing the four 2D simulations with the four 3D simulations is 49.3 %. This clearly indicates that the relation between the out-flowrate and the effective ventilation is the same for both simulations domains.

6 Assessment of the work done

6.1 Objectives Achieved

The main objective of this work was to study natural ventilation using Computation Fluid Dynamics (CFD). The work focused on ventilation in a classroom context, but, due to the very complex nature of the problem, this dissertation presented some preliminary studies for a case study of real classroom from a school in the metropolitan area of Porto, Portugal.

In the scope of this dissertation, both 2D and 3D CFD domains were made to study natural ventilation. The simulation setup and its effect on the converged solution were analysed, obtaining independent solutions

With this work, the ventilation through a window was studied: the flow structure and ventilation power. The effect of several design parameters was studied for the optimization of wind-driven ventilation in a classroom.

The ventilation efficiency was analysed using tracer simulations, and some insight into the nature and some problems of the renewal of indoor air were obtained.

6.2 Future Work

As mentioned before, the work developed in this thesis serves as a preliminary study for a case of real classroom. With this study, some previous characteristics could be studied, namely, the effect of multiple openings on the same room, a typical situation found in most classrooms, and not very studied by the scientific community yet.

Moreover, within the scope of the case study the effect of furniture, like tables and school cabinets, on the flow structure in the room and so on the ventilation can also be analysed.

The body of CFD work in this dissertation could be extended to increase available data, enabling the development of models that predict the ventilation rate from geometry and environmental parameter of a classroom. Furthermore, as mentioned in this thesis, the relation between some results of the 2D and 3D simulation, namely the $\%Q_{eff}$, could be further investigated to develop a way to use 2D simulations to study 3D ventilation.

7 References

Allocca, Camille, Qingyan Chen, and Leon R. Glicksman. 2003. "Design analysis of single-sided natural ventilation." *Energy and Buildings* 35 (8):785-795. doi: https://doi.org/10.1016/S0378-7788(02)00239-6.

ANSYS, Inc. 2022. *Ansys Fluent User Guide*.

Baetke, Frank, Heinrich Werner, and Hans Wengle. 1990. "Numerical simulation of turbulent flow over surface-mounted obstacles with sharp edges and corners." *Journal of Wind Engineering and Industrial Aerodynamics* 35:129-147. doi: https://doi.org/10.1016/0167-6105(90)90213-V.

Batterman, Stuart. 2017. "Review and Extension of CO_2-Based Methods to Determine Ventilation Rates with Application to School Classrooms." *International journal of environmental research and public health* 14 (2):145. doi: https://doi.org/10.3390/ijerph14020145.

Blocken, Bert, Ted Stathopoulos, and Jan Carmeliet. 2007. "CFD simulation of the atmospheric boundary layer: wall function problems." *Atmospheric Environment* 41 (2):238-252. doi: https://doi.org/10.1016/j.atmosenv.2006.08.019.

Chu, Chia-Ren, and Bo-Fan Chiang. 2014. "Wind-driven cross ventilation in long buildings." *Building and Environment* 80:150-158. doi: https://doi.org/10.1016/j.buildenv.2014.05.017.

Chu, Chia-Ren, Y. H. Chiu, Yi-Ting Tsai, and Si-Lei Wu. 2015. "Wind-driven natural ventilation for buildings with two openings on the same external wall." *Energy and Buildings* 108:365-372. doi: https://doi.org/10.1016/j.enbuild.2015.09.041.

CIBSE. 2000. ECG19 Energy Use in Offices - ECON19, ECON 19, ECG 19.

Cockroft, J. P., and P. Robertson. 1976. "Ventilation of an enclosure through a single opening." *Building and Environment* 11 (1):29-35. doi: https://doi.org/10.1016/0360-1323(76)90016-0.

EPE, Parque Escolar. 2017. Especificações Técnicas de Arquitetura para Projeto do edifício Escolar. https://parque-escolar.pt/docs/site/pt/programa/Parque-Escolar-Manual-Especificacoes-Tecnicas-Arquitetura.pdf.

Evola, G., and V. Popov. 2006. "Computational analysis of wind driven natural ventilation in buildings." *Energy and Buildings* 38 (5):491-501. doi: https://doi.org/10.1016/j.enbuild.2005.08.008.

Fadaei, Abdolmajid. 2021. "Ventilation Systems and COVID-19 Spread: Evidence from a Systematic Review Study." *European Journal of Sustainable Development Research* 5:em0157. doi: 10.21601/ejosdr/10845.

Fordham, M. 2000. "Natural ventilation." *Renewable Energy* 19 (1):17-37. doi: https://doi.org/10.1016/S0960-1481(99)00012-9.

Franke, Jörg, Charles Hirsch, A. Jensen, Henk Krüs, Michael Schatzmann, P. Westbury, S. Miles, J. Wisse, and Nigel Wright. 2004. "Recommendations on the use of CFD in wind engineering." *Proceedings of the International Conference on Urban Wind Engineering and Building Aerodynamics*. https://www.researchgate.net/publication/251814717_Recommendations_on_the_use_of_CFD_in_wind_engineering.

GMAO, Global Modeling and Assimilation Office. 2022. "Modern-Era Retrospective analysis for Research and Applications, Version 2." Last Modified 01/06/2022. https://gmao.gsfc.nasa.gov/reanalysis/MERRA-2/citing_MERRA-2/.

Hall, R.C. 1997. Evaluation of modelling uncertainty. CFD modelling of near-field atmospheric dispersion.: European Commission Directorate-General XII Science. https://www.inderscienceonline.com/doi/abs/10.1504/IJEP.2000.000526

Ji, Liang, Hongwei Tan, Shinsuke Kato, Zhen Bu, and Takeo Takahashi. 2011. "Wind tunnel investigation on influence of fluctuating wind direction on cross natural ventilation." *Building and Environment* 46 (12):2490-2499. doi: https://doi.org/10.1016/j.buildenv.2011.06.006.

Jiang, Yi, Donald Alexander, Huw Jenkins, Rob Arthur, and Qingyan Chen. 2003. "Natural ventilation in buildings: measurement in a wind tunnel and numerical simulation with large-eddy simulation." *Journal of Wind Engineering and Industrial Aerodynamics* 91 (3):331-353. doi: https://doi.org/10.1016/S0167-6105(02)00380-X.

Kato, Shinsuke, Ryohei Kono, Takamasa Hasama, Ryozo Ooka, and Takeo Takahashi. 2006. "A Wind Tunnel Experimental Analysis of the Ventilation Characteristics of a Room with Single-Sided Opening in Uniform Flow." *International Journal of Ventilation* 5 (1):171-178. doi: https://doi.org/10.1080/14733315.2006.11683734.

Larsen, Tine S., and Per Heiselberg. 2008. "Single-sided natural ventilation driven by wind pressure and temperature difference." *Energy and Buildings* 40 (6):1031-1040. doi: https://doi.org/10.1016/j.enbuild.2006.07.012.

Launder, B. E. Spalding D. B. 1972. *Lectures in mathematical models of turbulence*. London; New York: Academic Press ISBN: 0124380506 9780124380509.

Megahed, Naglaa A., and Ehab M. Ghoneim. 2021. "Indoor Air Quality: Rethinking rules of building design strategies in post-pandemic architecture." *Environmental Research* 193:110471. doi: https://doi.org/10.1016/j.envres.2020.110471.

Ministérios do Ambiente, Ordenamento do Território e Energia, da Saúde e da Solidariedade, Emprego e Segurança Social. 2021. Portaria n.º 138-G/2021. Diário da República n.º 126/2021, 2º Suplemento, Série I de 2021-07-01, páginas 2- 6.

Oropeza-Perez, Ivan, and Poul Alberg Østergaard. 2014. "Energy saving potential of utilizing natural ventilation under warm conditions – A case study of Mexico." *Applied Energy* 130:20-32. doi: https://doi.org/10.1016/j.apenergy.2014.05.035.

Petersen, S., K. L. Jensen, A. L. S. Pedersen, and H. S. Rasmussen. 2016. "The effect of increased classroom ventilation rate indicated by reduced CO2 concentration on the performance of schoolwork by children." *Indoor Air* 26 (3):366-379. doi: https://doi.org/10.1111/ina.12210.

Reynolds, William C. 1987. "Fundamentals of Turbulence for Turbulence Modeling and Simulation. https://www.semanticscholar.org/paper/Fundamentals-of-Turbulence-for-Turbulence-Modeling-Reynolds/54a89c5b8c2939a51f3b9a511ebafb75460d64a4."

Wang, Haojie, and Qingyan Chen. 2012. "A new empirical model for predicting single-sided, wind-driven natural ventilation in buildings." *Energy and Buildings* 54:386-394. doi: https://doi.org/10.1016/j.enbuild.2012.07.028.

Warren, P. R. 1977. "Ventilation through openings on one wall only." *Energy Conservation in Heating, Cooling, and Ventilation of Buildings* (1):189-209.

Warren, Philip R., and Lorna Parkins. 2013. "Single-sided Ventilation through open windows https://www.semanticscholar.org/paper/SINGLE-SIDED-VENTILATION-THROUGH-OPEN-WINDOWS-Warren-Parkins/4ec800564710062915e8e28815f11853859cad1e."

Weerasuriya, A. U., Xuelin Zhang, Vincent J. L. Gan, and Yi Tan. 2019. "A holistic framework to utilize natural ventilation to optimize energy performance of residential high-rise

buildings." *Building and Environment* 153:218-232. doi: https://doi.org/10.1016/j.buildenv.2019.02.027.

Yik, Francis W. H., and Lun Yu Fat. 2010. "Energy Saving by Utilizing Natural Ventilation in Public Housing in Hong Kong." *Indoor and Built Environment* 19 (1):73-87. doi: https://doi.org/10.1177/1420326X09358021.

Zhang, Xuelin, A. U. Weerasuriya, and K. T. Tse. 2020. "CFD simulation of natural ventilation of a generic building in various incident wind directions: Comparison of turbulence modelling, evaluation methods, and ventilation mechanisms." *Energy and Buildings* 229:110516. doi: https://doi.org/10.1016/j.enbuild.2020.110516.

Zhuang, Ruining, Xiangdong Li, and Jiyuan Tu. 2014. "CFD study of the effects of furniture layout on indoor air quality under typical office ventilation schemes." *Building Simulation* 7. doi: https://doi.org/10.1007/s12273-013-0144-5.

Appendix A - Extra Tracer Simulation

In this appendix the results from some extra tracer simulations both 3D and 2D are presented.

The simulations are identical to the one described in the main text, sections 3.3 and 4.3, changing only the initial concentration of CO_2, namely 0.003 and 0.025. For every group of simulation, a single concentration history is presented. The results of the considered ventilation metrics are presented in tables.

1: $x_{CO2}^{0} = 0.025$

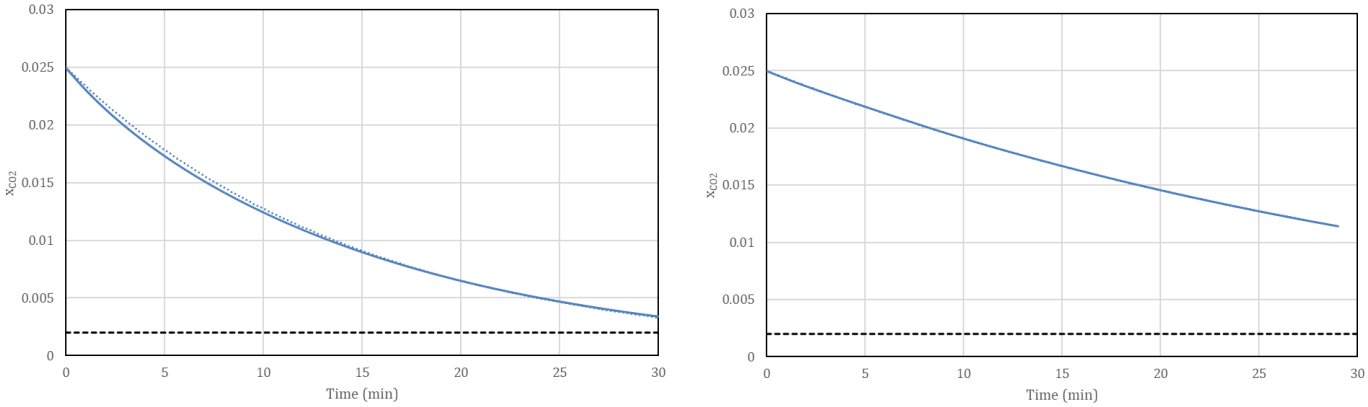


Figure 39. Average CO_2 mass fraction history for the base case, . $U = 5\ km\ h^{-1}$ and $w = 0.6\ m$, and an initial concentration of 0.025 from a 2D simulation (right) and a 3D simulation (left)

Table 8. Tracer results for an initial concentration of 0.025

	Condition	τ_{vent} (min)	$\%Q_{eff}$	$\%vent$
2D	Base Case: $U = 5\ \mathrm{km\ h^{-1}}$ $w = 0.6\ \mathrm{m}$	14.70	20.9	86.5
	$U = 9\ \mathrm{km\ h^{-1}}$	8.85	19.5	96.6
	$w = 1.5\ \mathrm{m}$	5.81	18.0	99.4
3D	Base Case	37.04	41.6	55.5
	$U = 9\ \mathrm{km\ h^{-1}}$	20.00	44.4	77.7
	$w = 1.5\ \mathrm{m}$	6.15	35.2	99.2

2: $x_{CO2}^{0} = 0.003$

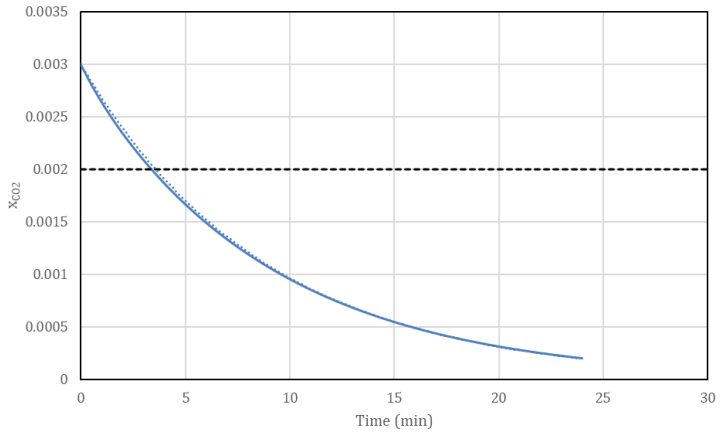


Figure 40 Average CO_2 mass fraction history for from a 2D simulation and an initial concentration of 0.003. $U = 9\ km\ h^{-1}$ and $w = 0.6\ m$

Table 9. 2D tracer results for an initial concentration of 0.003

Condition	τ_{vent} (min)	$\%Q_{eff}$	$\%vent$
Base Case: $U = 5\ \mathrm{km\ h^{-1}}$ $w = 0.6\ \mathrm{m}$	14.70	20.9	86.5
$U = 9\ \mathrm{km\ h^{-1}}$	8.85	19.5	96.6
$w = 1.5\ \mathrm{m}$	5.81	18.0	99.4

Appendix B – Exterior Flow Structure

To visualize the flow structure outside the building, pathlines were plotted in the base 3D case ($w = 0.6$ m and $U = 5$ km s^{-1}). Figure 41, Figure 42 and Figure 43 show this flow from different angles. Similar to what was described for the 2D case, using the streamline plots, the air mainly flows through the top of the building creating a curve, similar to a bump. At the back of the building, a more turbulent flow can be notice existing circulation zones. From the back view, two spiral channels can be discerned. Figure 45 shows the pathlines originating from the window. From these figures it is clear to see that the flow isn't fully symmetrical in all of the domain confirming the convergence issues present with the half domain model.

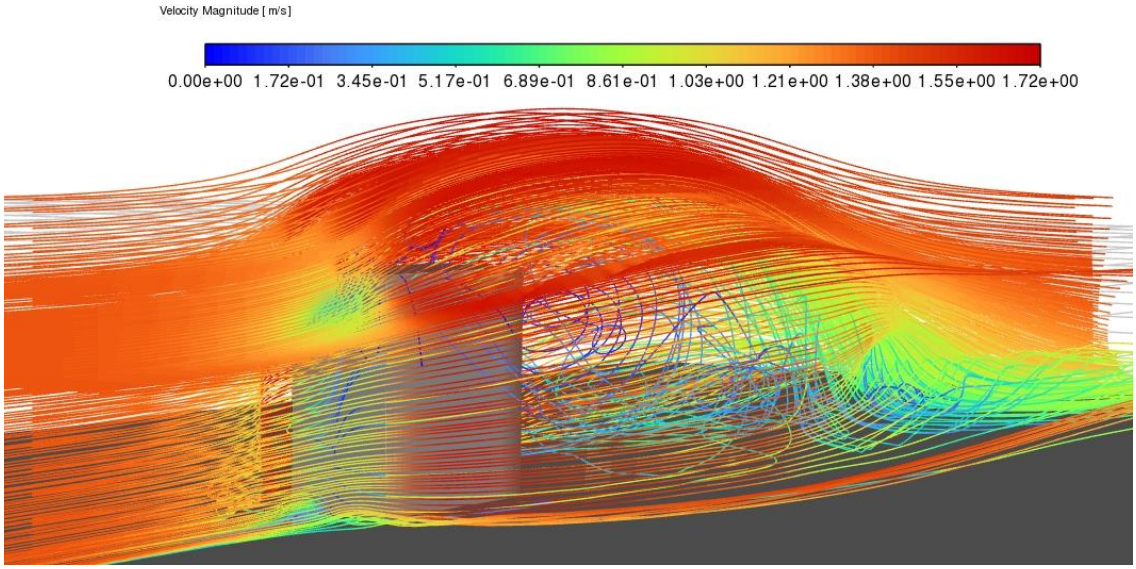


Figure 41. Front view of pathlines coloured by velocity magnitude for the 3D simulation ($w = 0.6\ m$ and $U = 5\ km\ s^{-1}$)

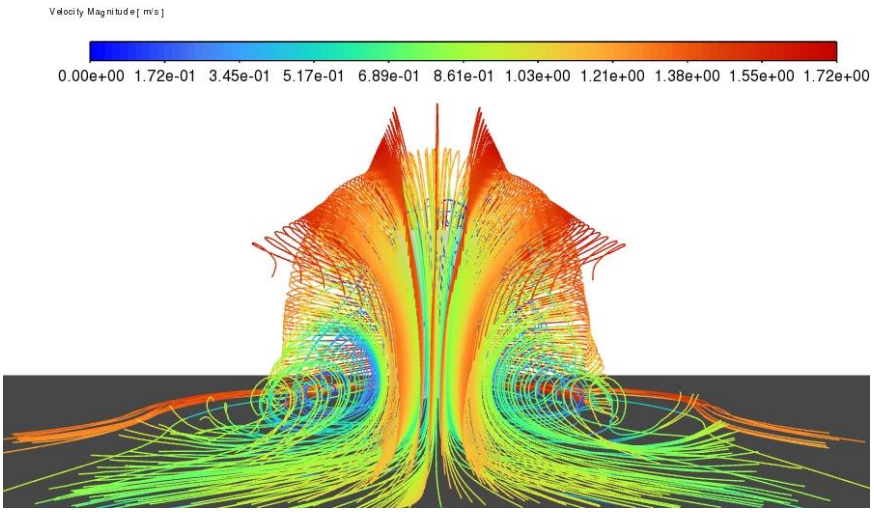


Figure 42. Back view of pathlines coloured by velocity magnitude for the 3D simulation ($w = 0.6\ m$ and $U = 5\ km\ s^{-1}$)

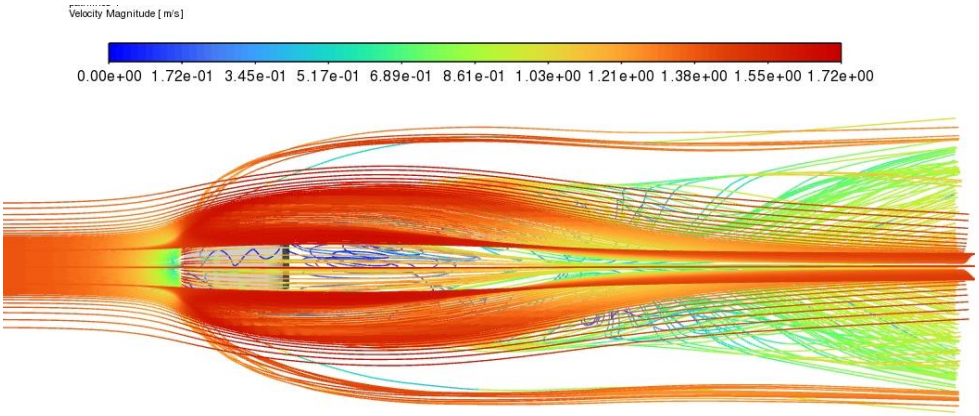


Figure 43. Top view of pathlines coloured by velocity magnitude for the 3D simulation ($w = 0.6\ m$ and $U = 5\ km\ s^{-1}$)

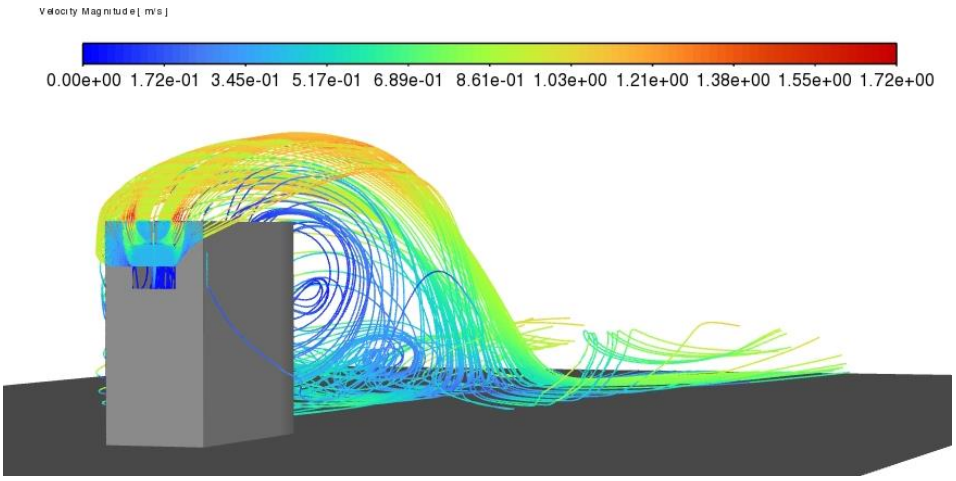


Figure 44. Pathlines originating from the opening of the room coloured by velocity magnitude for the 3D simulation ($w = 0.6\ m$ and $U = 5\ km\ s^{-1}$)